Compositional control of pore geometry in multivariate metal-organic frameworks: an experimental and computational study

Laura K. Cadman, Jessica K. Bristow, Naomi E. Stubbs, Davide Tiana, Mary F. Mahon* Aron Walsh* and Andrew D. Burrows*

Supporting Information

1. General experimental details
2. Synthetic procedures
3. Compound list
4. NMR studies
5. Powder X-ray diffraction studies
6. X-ray crystallography
7. Computational studies
8. References

1. General experimental details

With the exception of 2-iodo-1,4-benzenedicarboxylic acid (H_2bdc-I), starting materials and solvents were purchased from commercial sources and were used without further purification.

Powder X-ray diffraction (PXRD) patterns were recorded on a Bruker AXS D8 Advance diffractometer with copper Kα radiation of wavelength 1.5406 Å at 298 K. Samples were placed on a flat plate, and measured with a 2θ range of 5-60°. The step size was 0.024° with time per step of 0.3 s. Samples for PXRD analysis were air dried at room temperature for 1-2 minutes.

^{1}H NMR spectroscopy on bulk samples was carried out on a 300 MHz Bruker Avance Spectrometer. Samples were dried at 100°C for 20 minutes and digested in a solution of DMSO-d_6 and DCl. The digestion solution was prepared by combining 3 ml DMSO-d_6 with 0.1 ml DCl (35% wt in D_2O). Each sample was dissolved in 0.4 ml of DMSO-d_6 and 0.2 ml of the digestion solution. ^{1}H NMR spectroscopy on individual crystals was carried out on a 500 MHz Bruker Avance using a dual solvent suppression programme. Samples were prepared in the same way as the bulk NMR samples.

TGA experiments were carried out on a Perkin Elmer TGA 4000 Thermogravimetric Analyser. The samples were heated from 25°C to 600°C at a heating rate of 10°C/min, under a flow of nitrogen (20 mL/min).

2. Synthetic procedures

H_2bdc-I was prepared according to previously reported methods.[S1] Synthesis of the mixed-linker compounds in series **1-5** were carried out using an analogous synthesis to that of DMOF-1, originally reported by Kim and co-workers.[S2] A typical synthesis (for **1a**) is described below.

2.1 Synthesis of [Zn_2(bdc)(bdc-Br)(dabco)]·DMF, 1a

$Zn(NO_3)_2·6H_2O$ (0.50 mmol, 0.149 g), H_2bdc (0.40 mmol, 0.067 g), H_2bdc-Br (0.10 mmol, 0.025 g) and dabco (0.25 mmol, 0.028 g) were dissolved in 7 ml anhydrous DMF. The solution was placed in a glass vial and sealed. The sample was sonicated for 10-15 minutes to fully dissolve the reagents and heated at 120°C for 3 days. Colourless, block shaped crystals were collected and washed 2-3 times with fresh DMF. The product was analysed by ^{1}H NMR spectroscopy and PXRD.

Other synthesis were carried out in an analogous manner, using a total of 0.50 mmol of the two dicarboxylic acids.

3. Compound List

The average formula of all compounds synthesised are given in the table below. The formulae were established through ^{1}H NMR studies, where an average of bulk and individual crystal NMR integral analysis were used to determine the dicarboxylate ratios.

Series and General Formula	**Average Compound Formula (as determined through ^{1}H NMR studies)**
1 $[Zn_2(bdc)_{2-x}(bdc\text{-}Br)_x(dabco)]$	$[Zn_2(bdc)_{1.7}(bdc\text{-}Br)_{0.3}(dabco)]\cdot n$DMF
	$[Zn_2(bdc)_{1.44}(bdc\text{-}Br)_{0.56}(dabco)]\cdot n$DMF
	$[Zn_2(bdc)_{1.36}(bdc\text{-}Br)_{0.64}(dabco)]\cdot n$DMF
	$[Zn_2(bdc)_{1.25}(bdc\text{-}Br)_{0.75}(dabco)]\cdot n$DMF
	$[Zn_2(bdc)_{1.2}(bdc\text{-}Br)_{0.8}(dabco)]\cdot n$DMF
	$[Zn_2(bdc)_{0.8}(bdc\text{-}Br)_{1.2}(dabco)]\cdot n$DMF
	$[Zn_2(bdc)_{0.67}(bdc\text{-}Br)_{1.33}(dabco)]\cdot n$DMF
	$[Zn_2(bdc)_{0.5}(bdc\text{-}Br)_{1.5}(dabco)]\cdot n$DMF
	$[Zn_2(bdc)_{0.3}(bdc\text{-}Br)_{1.7}(dabco)]\cdot n$DMF
2 $[Zn_2(bdc)_{2-x}(bdc\text{-}I)_x(dabco)]$	$[Zn_2(bdc)_{1.78}(bdc\text{-}I)_{0.22}(dabco)]\cdot n$DMF
	$[Zn_2(bdc)_{1.58}(bdc\text{-}I)_{0.42}(dabco)]\cdot n$DMF
	$[Zn_2(bdc)_{1.23}(bdc\text{-}I)_{0.77}(dabco)]\cdot n$DMF
	$[Zn_2(bdc)_{0.75}(bdc\text{-}I)_{1.25}(dabco)]\cdot n$DMF
3 $[Zn_2(bdc)_{2-x}(bdc\text{-}NO_2)_x(dabco)]$	$[Zn_2(bdc)_{1.79}(bdc\text{-}NO_2)_{0.21}(dabco)]\cdot n$DMF
	$[Zn_2(bdc)_{1.63}(bdc\text{-}NO_2)_{0.37}(dabco)]\cdot n$DMF
	$[Zn_2(bdc)_{1.42}(bdc\text{-}NO_2)_{0.58}(dabco)]\cdot n$DMF
	$[Zn_2(bdc)_{1.22}(bdc\text{-}NO_2)_{0.78}(dabco)]\cdot n$DMF
	$[Zn_2(bdc)_{1.2}(bdc\text{-}NO_2)_{0.8}(dabco)]\cdot n$DMF
	$[Zn_2(bdc)_{0.86}(bdc\text{-}NO_2)_{1.14}(dabco)]\cdot n$DMF
	$[Zn_2(bdc)_{0.46}(bdc\text{-}NO_2)_{1.54}(dabco)]\cdot n$DMF
	$[Zn_2(bdc)_{0.42}(bdc\text{-}NO_2)_{1.58}(dabco)]\cdot n$DMF
	$[Zn_2(bdc)_{0.29}(bdc\text{-}NO_2)_{1.71}(dabco)]\cdot n$DMF
4 $[Zn_2(bdc)_{2-x}(bdc\text{-}NH_2)_x(dabco)]$	$[Zn_2(bdc)_{1.84}(bdc\text{-}NH_2)_{0.16}(dabco)]\cdot n$DMF
	$[Zn_2(bdc)_{1.6}(bdc\text{-}NH_2)_{0.4}(dabco)]\cdot n$DMF
	$[Zn_2(bdc)_{1.49}(bdc\text{-}NH_2)_{0.51}(dabco)]\cdot n$DMF
	$[Zn_2(bdc)_{1.38}(bdc\text{-}NH_2)_{0.62}(dabco)]\cdot n$DMF

	$[Zn_2(bdc)_{1.12}(bdc\text{-}NH_2)_{0.88}(dabco)]\cdot n$DMF
	$[Zn_2(bdc)_{1.01}(bdc\text{-}NH_2)_{0.99}(dabco)]\cdot n$DMF
	$[Zn_2(bdc)_{0.67}(bdc\text{-}NH_2)_{1.33}(dabco)]\cdot n$DMF
	$[Zn_2(bdc)_{0.5}(bdc\text{-}NH_2)_{1.5}(dabco)]\cdot n$DMF
	$[Zn_2(bdc)_{0.2}(bdc\text{-}NH_2)_{1.8}(dabco)]\cdot n$DMF
5 $[Zn_2(bdc\text{-}Br)_{2-x}(bdc\text{-}I)_x(dabco)]$	$[Zn_2(bdc\text{-}Br)_{1.81}(bdc\text{-}I)_{0.19}(dabco)]\cdot n$DMF
	$[Zn_2(bdc\text{-}Br)_{1.4}(bdc\text{-}I)_{0.6}(dabco)]\cdot n$DMF
	$[Zn_2(bdc\text{-}Br)_{1.01}(bdc\text{-}I)_{0.99}(dabco)]\cdot n$DMF

4. NMR studies

The inclusion of bdc-X into series **1-5** was assessed by ^{1}H NMR spectroscopy. In all cases the % bdc-X (X = Br, I, NO_2, NH_2) included in the product was estimated using NMR integrals averaged over several samples and compared with the % bdc-X present in the reaction mixture. For series **5**, X = I. The results of the NMR analyses are summarised in Figure S1.

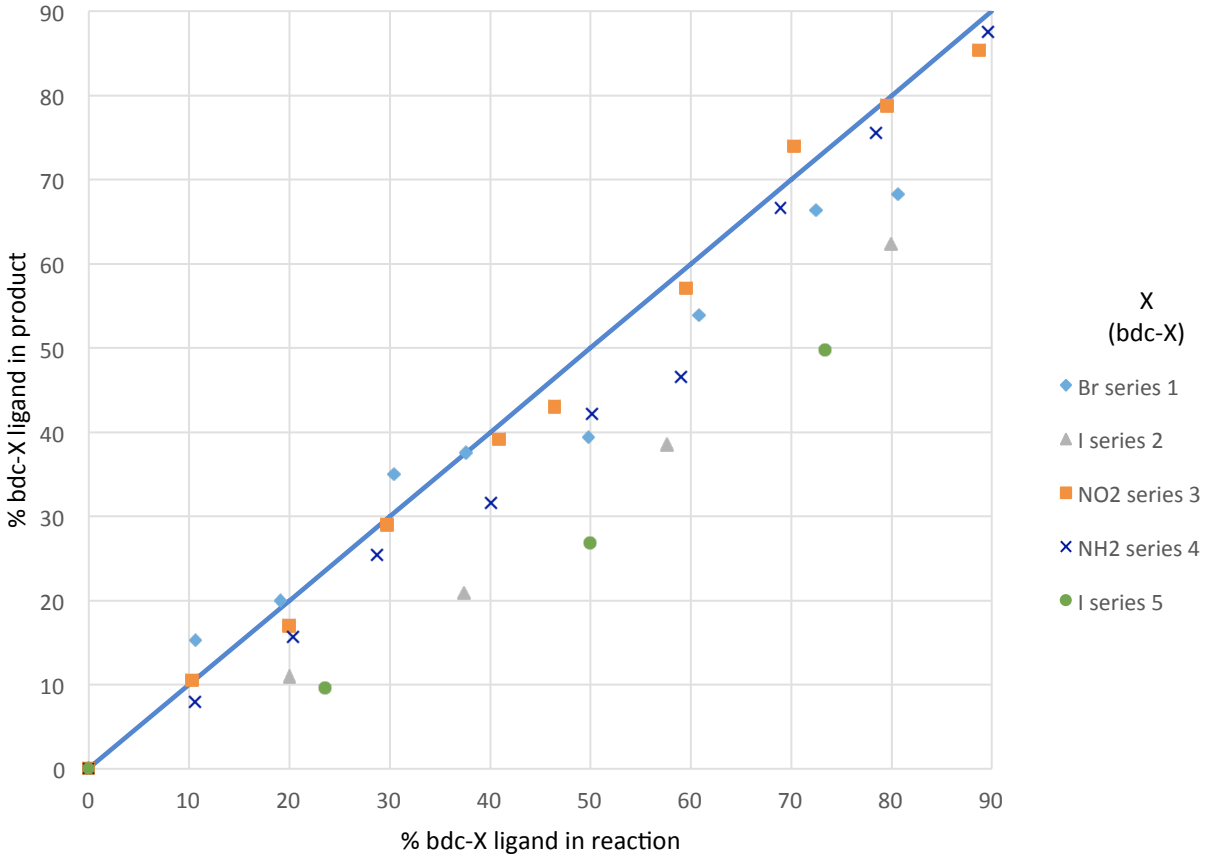

Figure S1. The inclusion of bdc-X into the product for series **1**, **2**, **3**, **4** and **5** as evidenced by NMR spectroscopy.

NMR data of series **1-5** showing bulk, filtered and individual crystal samples (where relevant) in a digested sample are shown in Figures S2-S18. Single crystal samples were carried out using one individual crystal of the product.

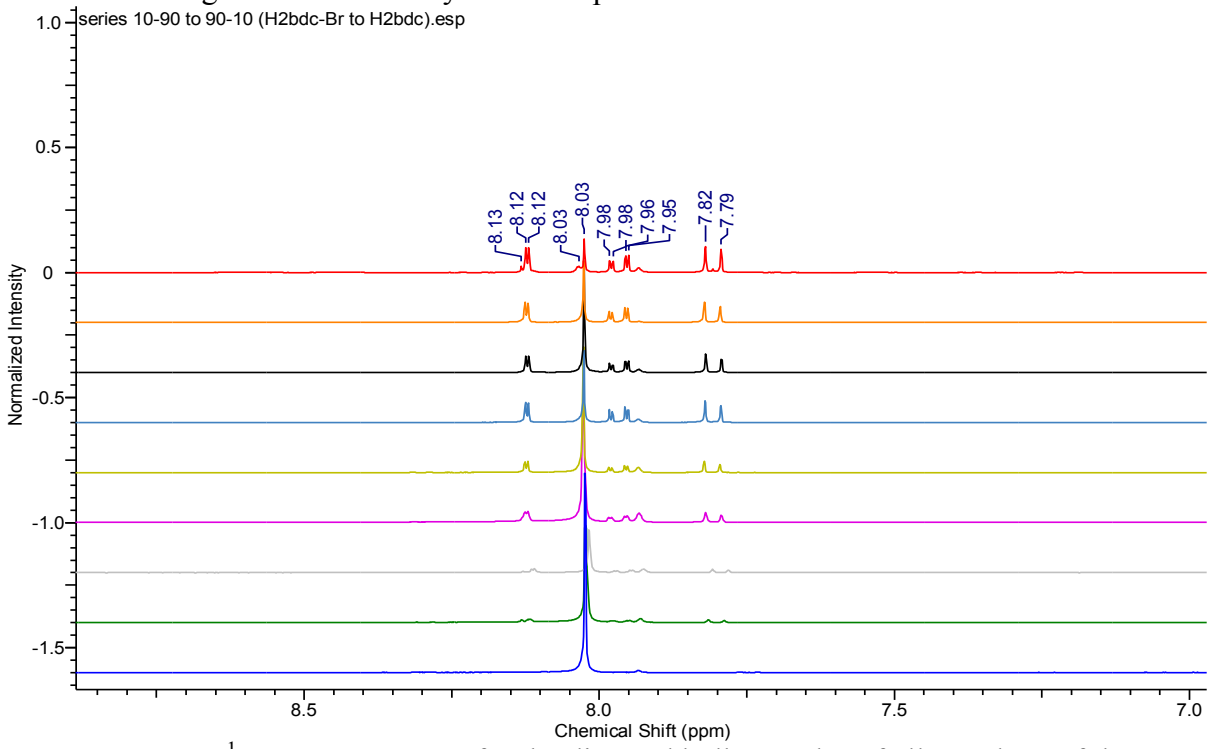

Figure S2. ^{1}H NMR spectrum for the digested bulk samples of all members of the $[Zn_2(bdc)_{2-x}(bdc\text{-}Br)_x(dabco)]\cdot n$DMF (**1**) series

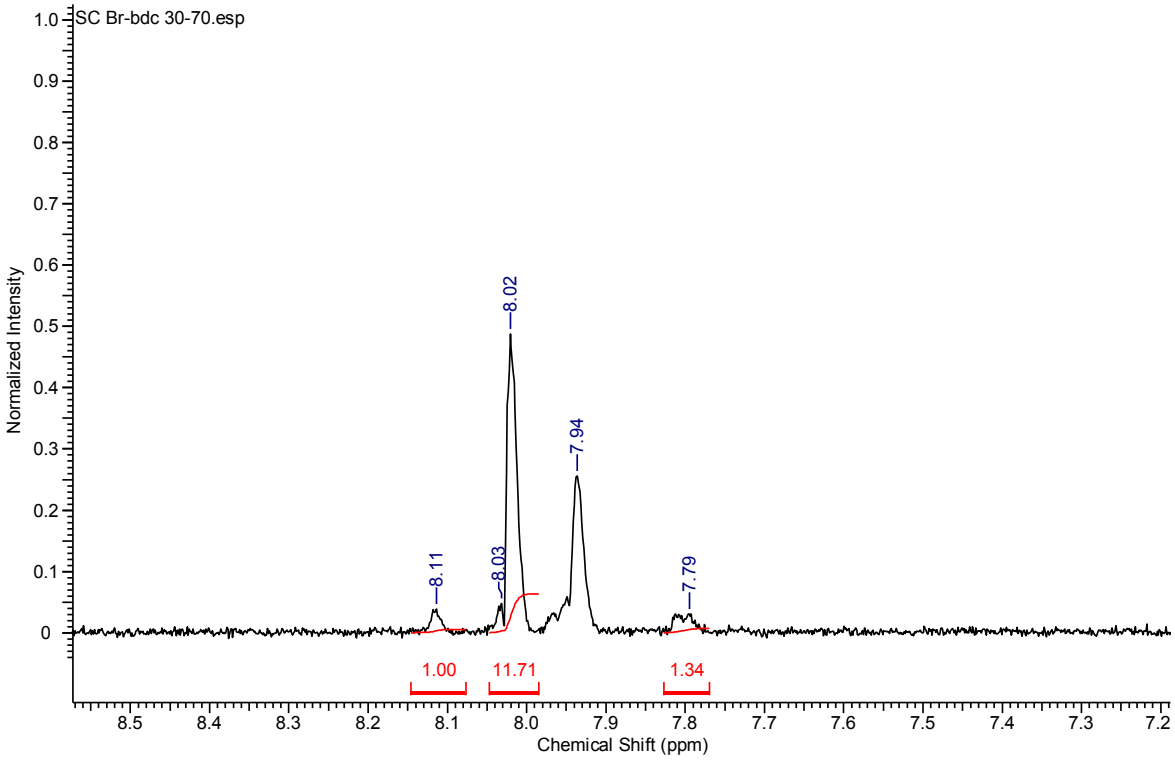

Figure S3. ^{1}H NMR spectrum for a digested single crystal sample of $[Zn_2(bdc)_{1.36}(bdc\text{-}Br)_{0.64}(dabco)]\cdot n$DMF

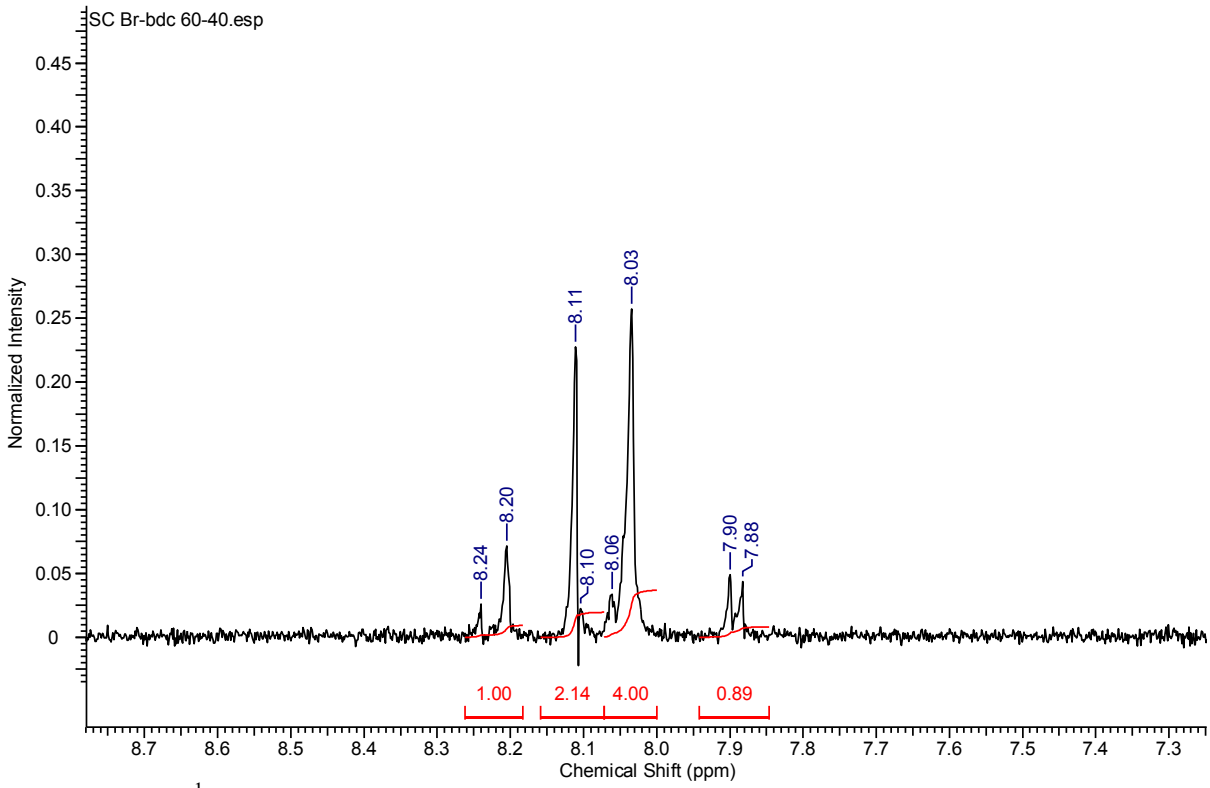

Figure S4. ^{1}H NMR spectrum for a digested single crystal sample of $[Zn_2(bdc)_{0.85}(bdc\text{-}Br)_{1.15}(dabco)]\cdot n$DMF

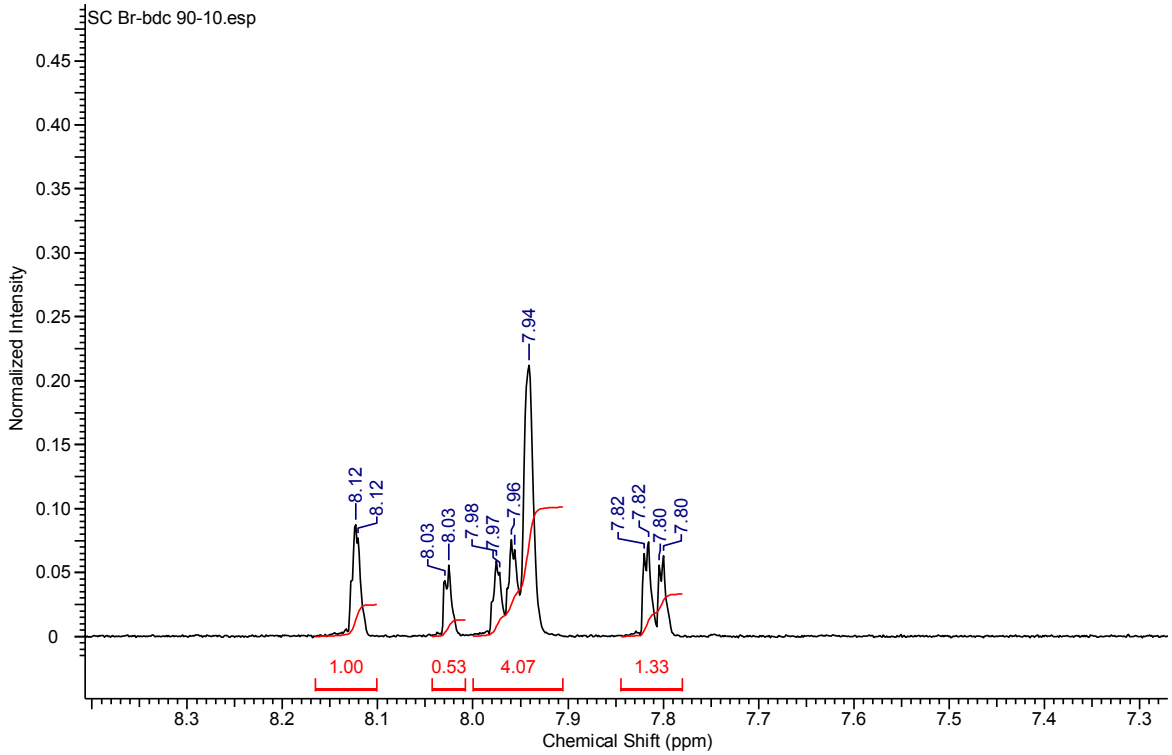

Figure S5. ^{1}H NMR spectrum for a digested single crystal sample of $[Zn_2(bdc)_{0.27}(bdc\text{-}Br)_{1.73}(dabco)]\cdot n$DMF

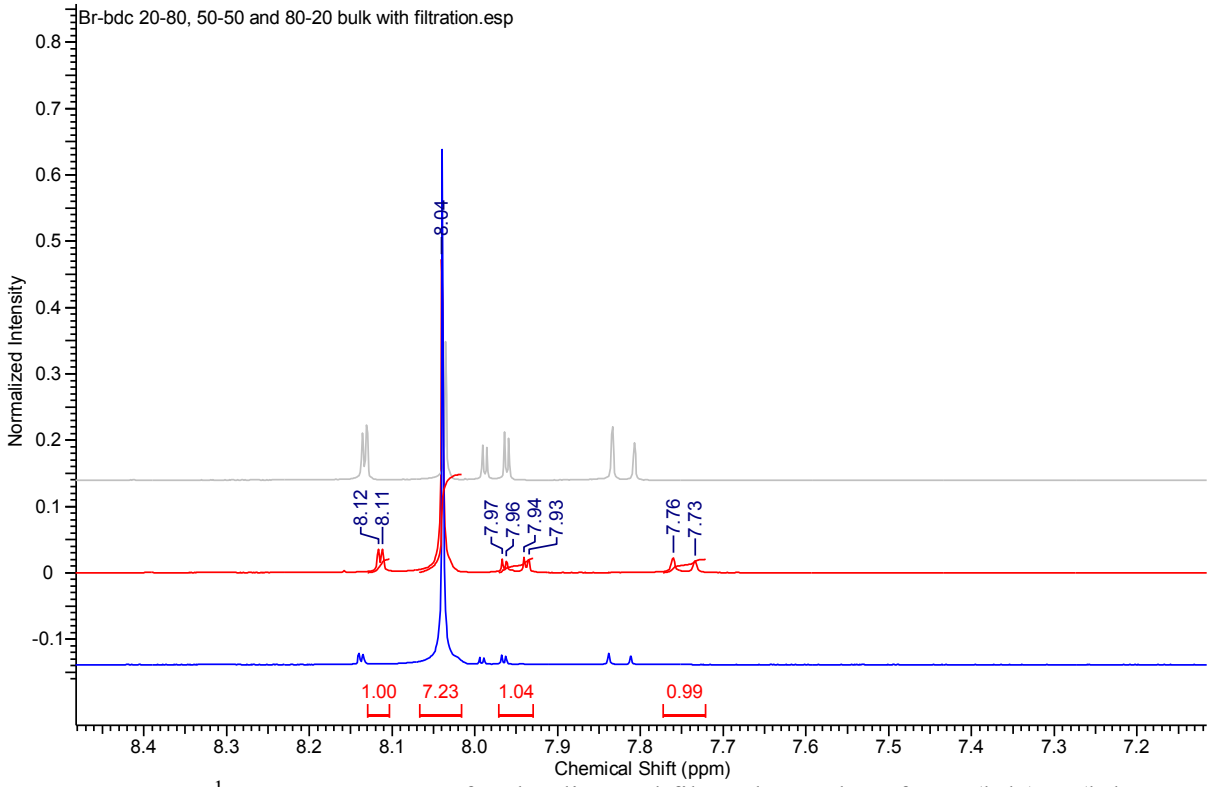

Figure S6. ^{1}H NMR spectrum for the digested filtered samples of $[Zn_2(bdc)_{1.44}(bdc\text{-}Br)_{0.56}(dabco)]\cdot n$DMF (bottom), $[Zn_2(bdc)_{1.21}(bdc\text{-}Br)_{0.79}(dabco)]\cdot n$DMF (middle) and $[Zn_2(bdc)_{0.56}(bdc\text{-}Br)_{1.44}(dabco)]\cdot n$DMF (top)

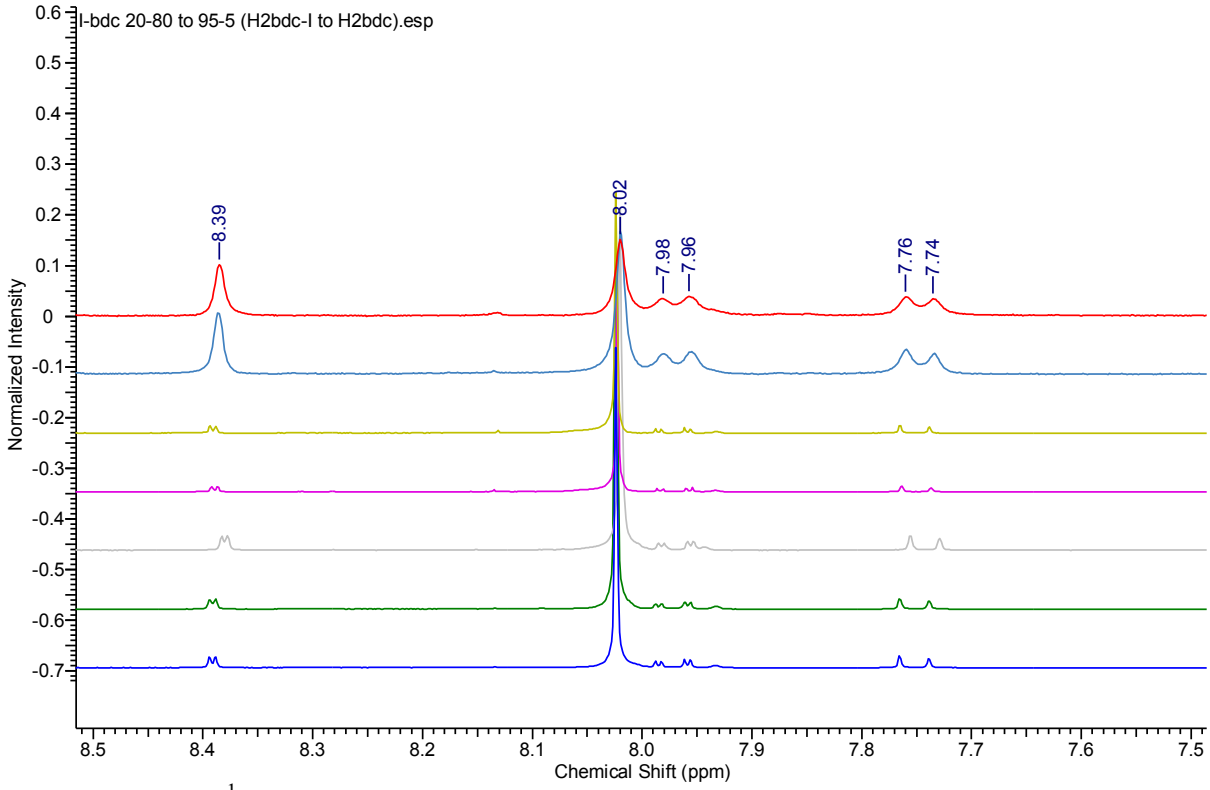

Figure S7. ^{1}H NMR spectrum for the digested bulk samples of all members of the $[Zn_2(bdc)_{2-x}(bdc\text{-}I)_x(dabco)]\cdot n$DMF (**2**) series

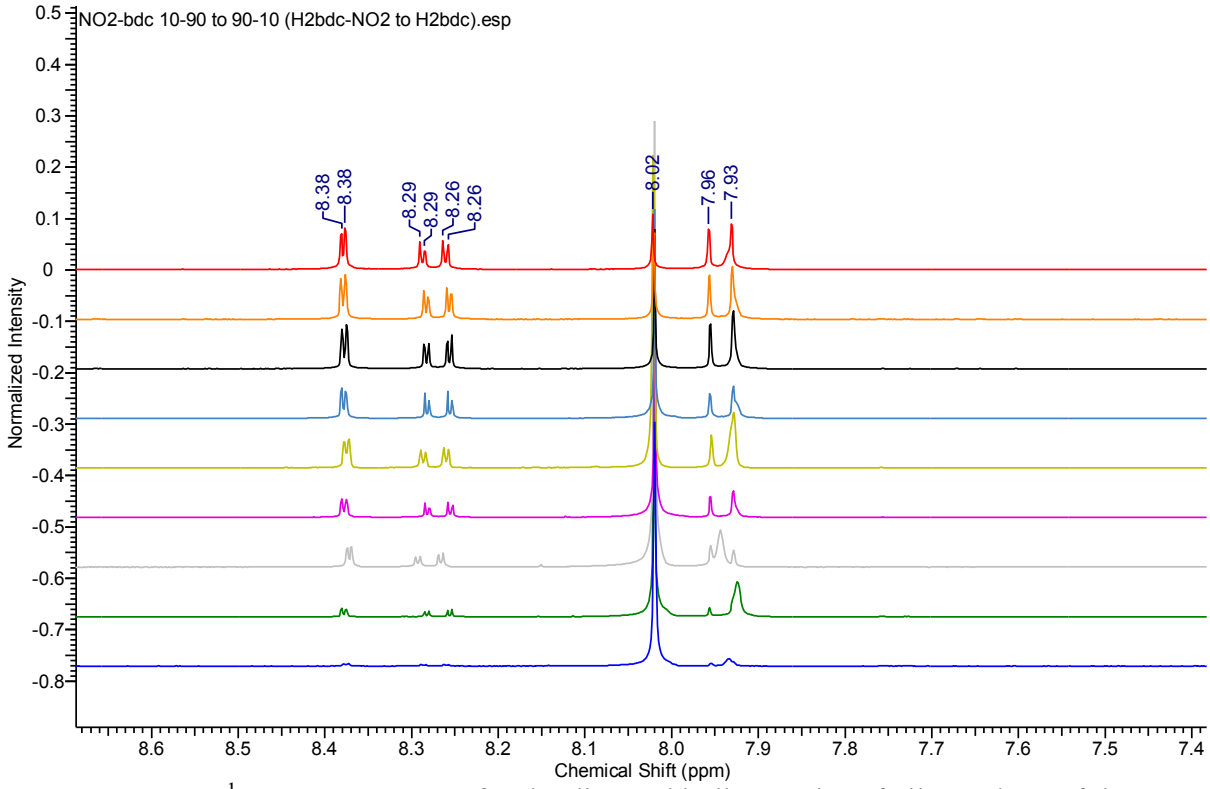

Figure S8. ^{1}H NMR spectrum for the digested bulk samples of all members of the $[Zn_2(bdc)_{2-x}(bdc\text{-}NO_2)_x(dabco)]\cdot n$DMF (**3**) series

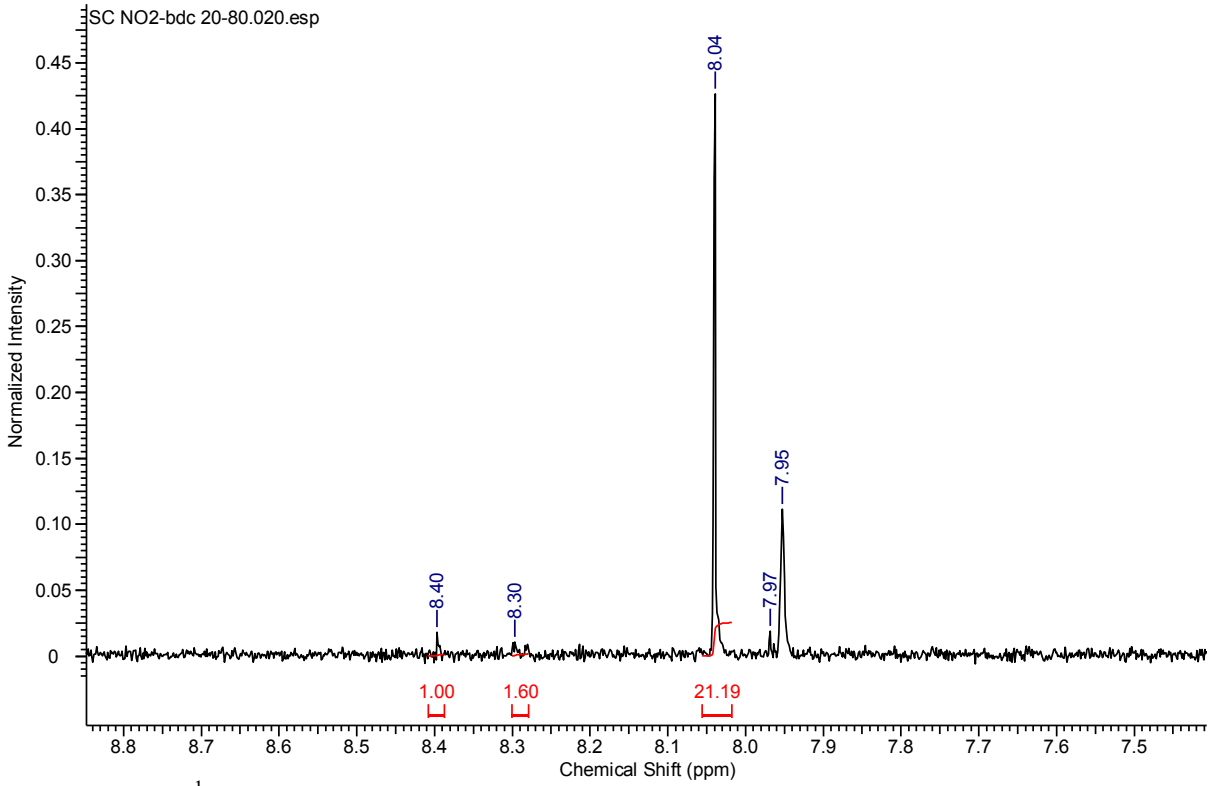

Figure S9. ^{1}H NMR spectrum for a digested single crystal sample of $[Zn_2(bdc)_{1.63}(bdc\text{-}NO_2)_{0.37}(dabco)]\cdot n$DMF

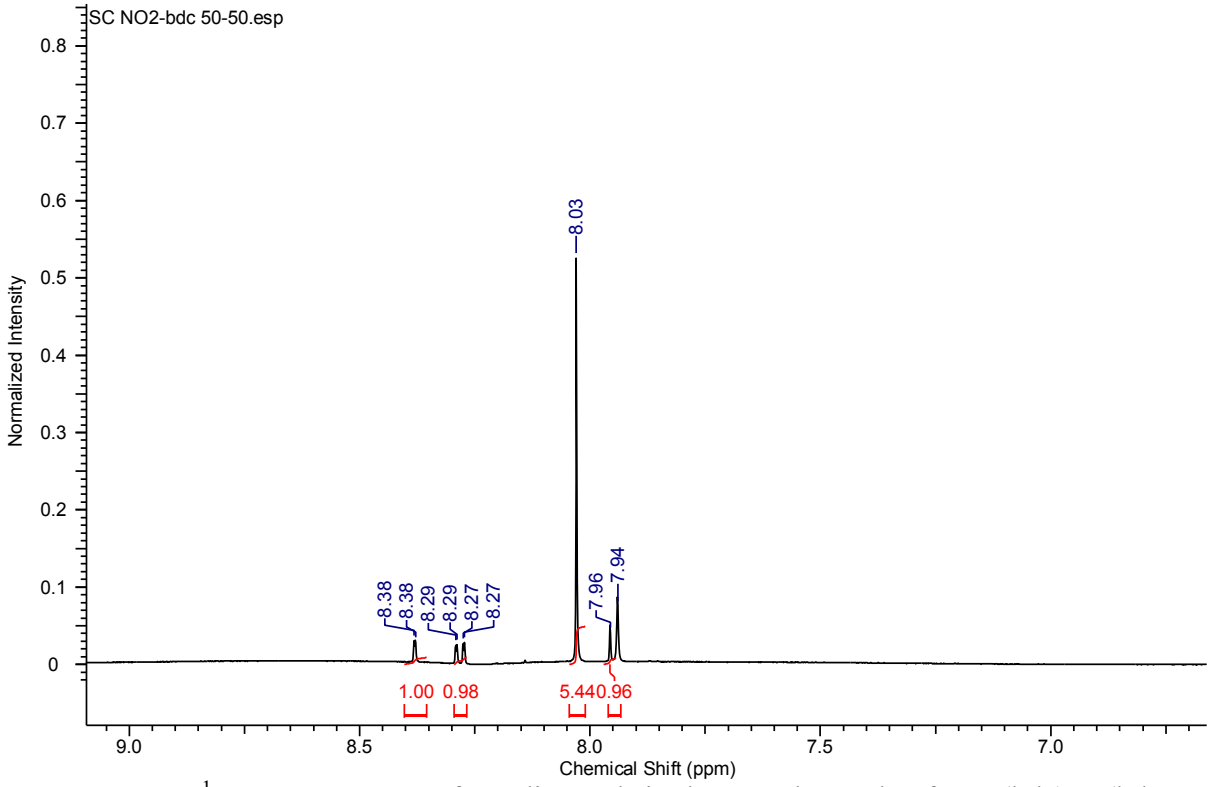

Figure S10. ^{1}H NMR spectrum for a digested single crystal sample of $[Zn_2(bdc)_{1.15}(bdc\text{-}NO_2)_{0.85}(dabco)]\cdot n$DMF

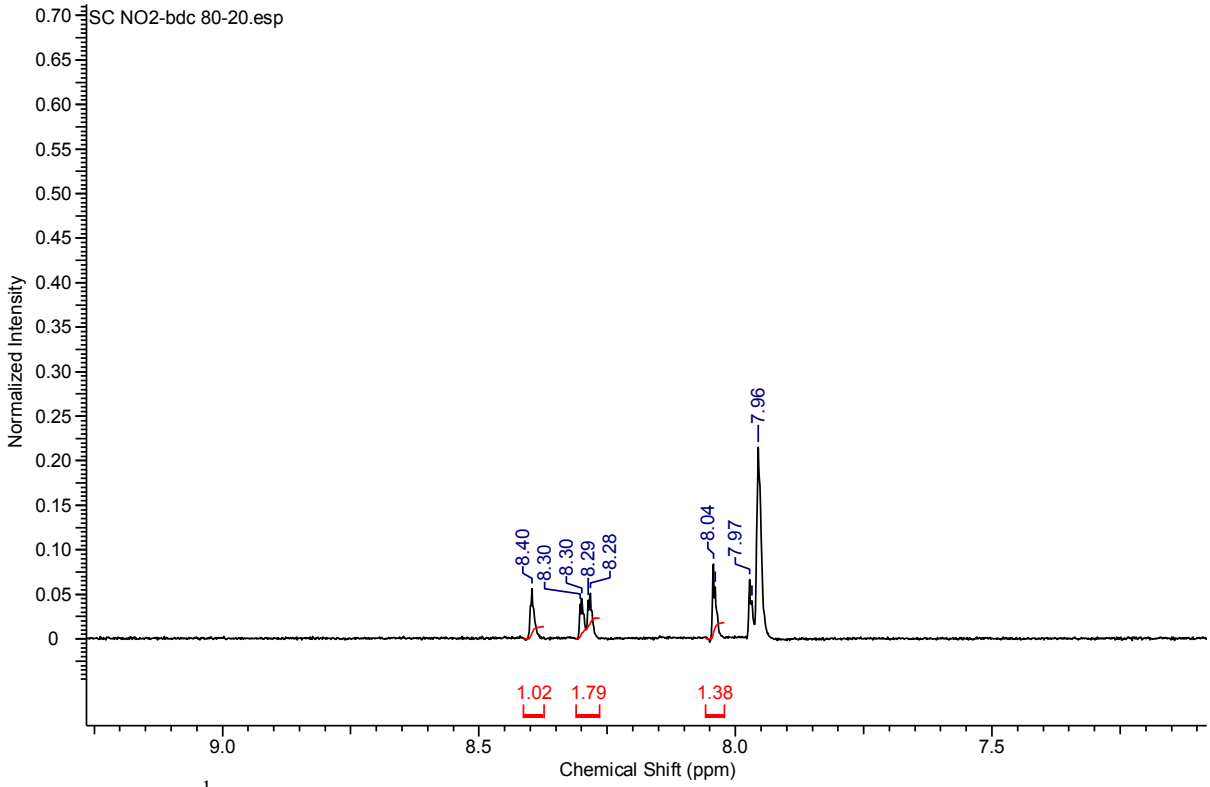

Figure S11. ^{1}H NMR spectrum for a digested single crystal sample of $[Zn_2(bdc)_{0.42}(bdc\text{-}NO_2)_{1.58}(dabco)]\cdot n$DMF

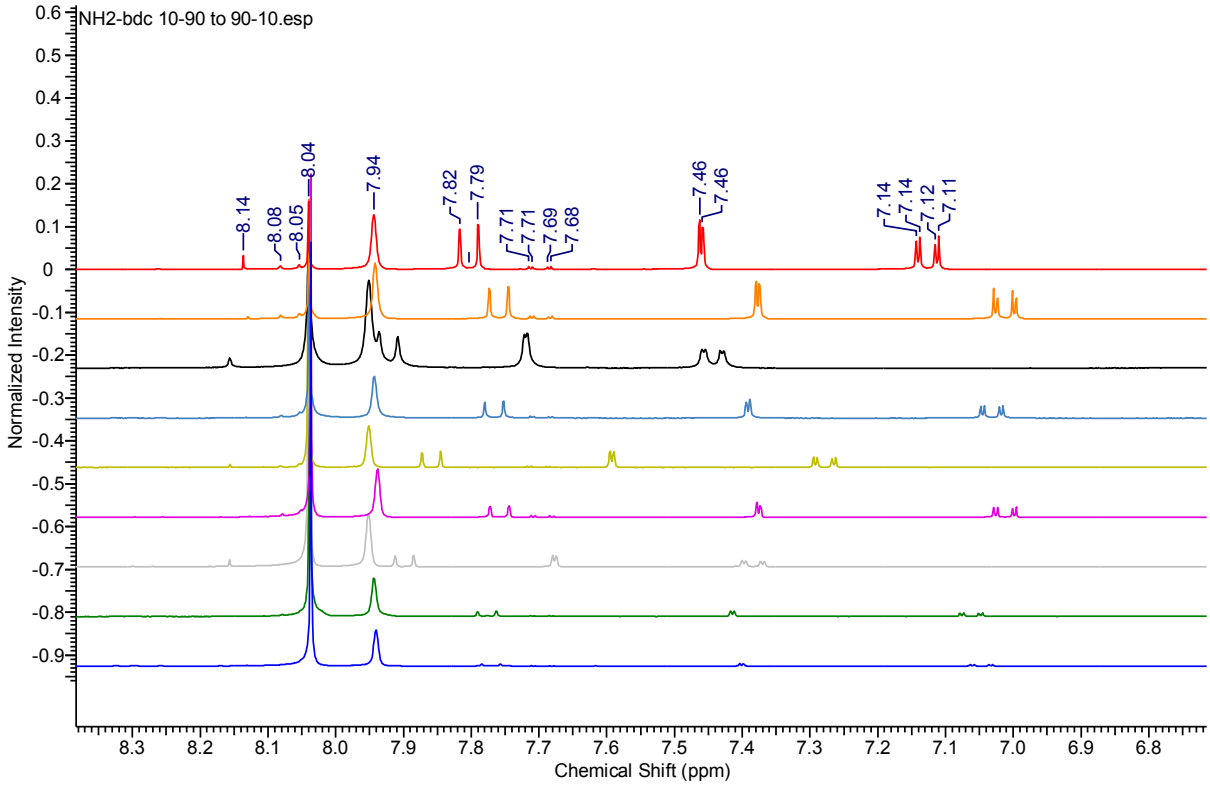

Figure S12. ^{1}H NMR spectrum for the digested bulk samples of all members of the $[Zn_2(bdc)_{2-x}(bdc\text{-}NH_2)_x(dabco)]\cdot n$DMF (**4**) series. The variation in chemical shift of H_2bdc-NH_2 is caused by protonation of the amino group by the digestion solution (DCl/dmso-d_6).

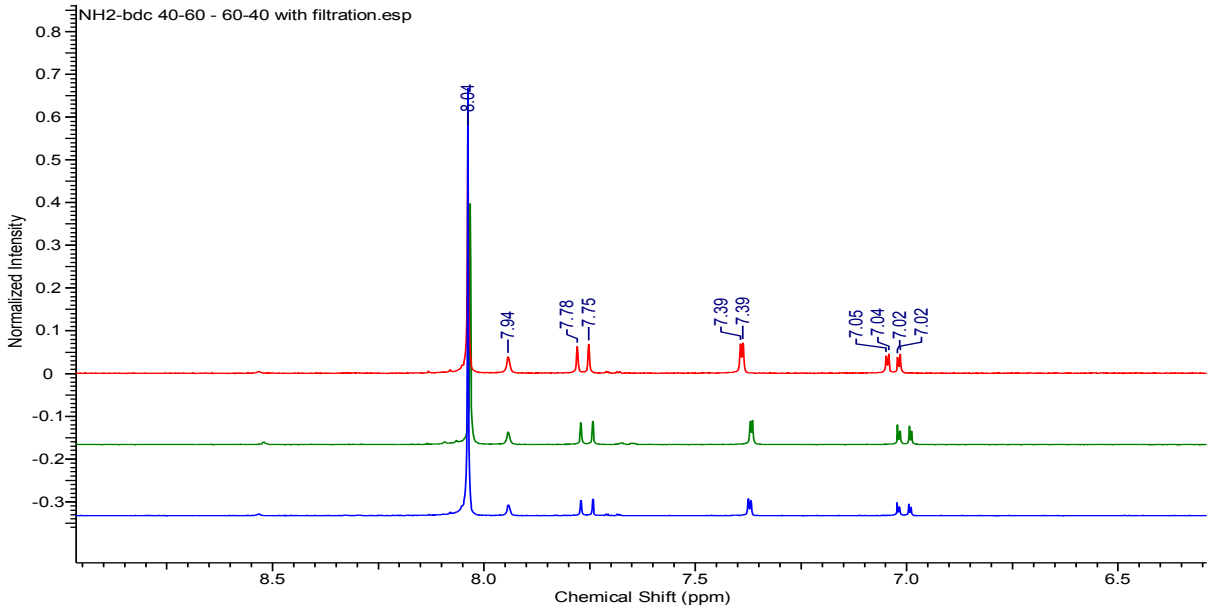

Figure S13. ^{1}H NMR spectrum for the digested filtered samples of $[Zn_2(bdc)_{1.38}(bdc\text{-}NH_2)_{0.62}(dabco)]\cdot n$DMF (bottom), $[Zn_2(bdc)_{1.12}(bdc\text{-}NH_2)_{0.88}(dabco)]\cdot n$DMF (middle) and $[Zn_2(bdc)_{1.01}(bdc\text{-}NH_2)_{0.99}(dabco)]\cdot n$DMF (top)

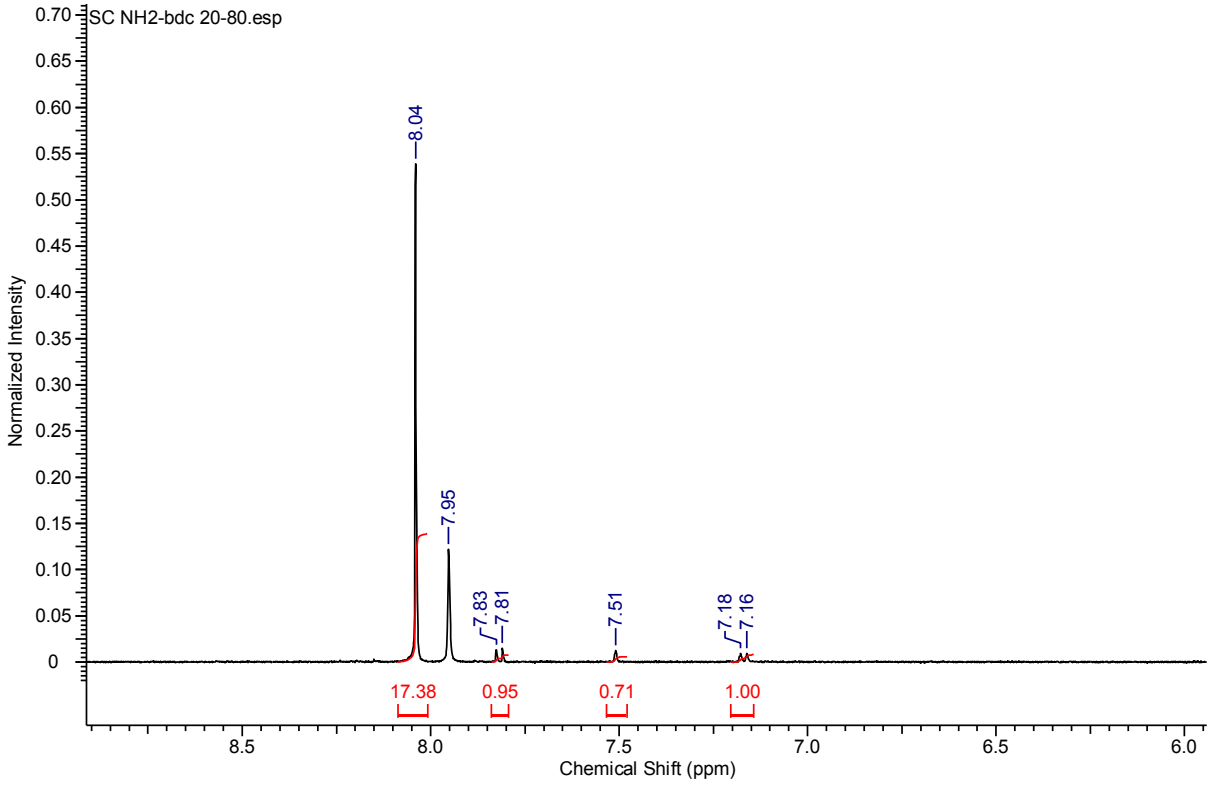

Figure S14. ^{1}H NMR spectrum for a digested single crystal sample of $[Zn_2(bdc)_{1.67}(bdc\text{-}NH_2)_{0.33}(dabco)]\cdot n$DMF

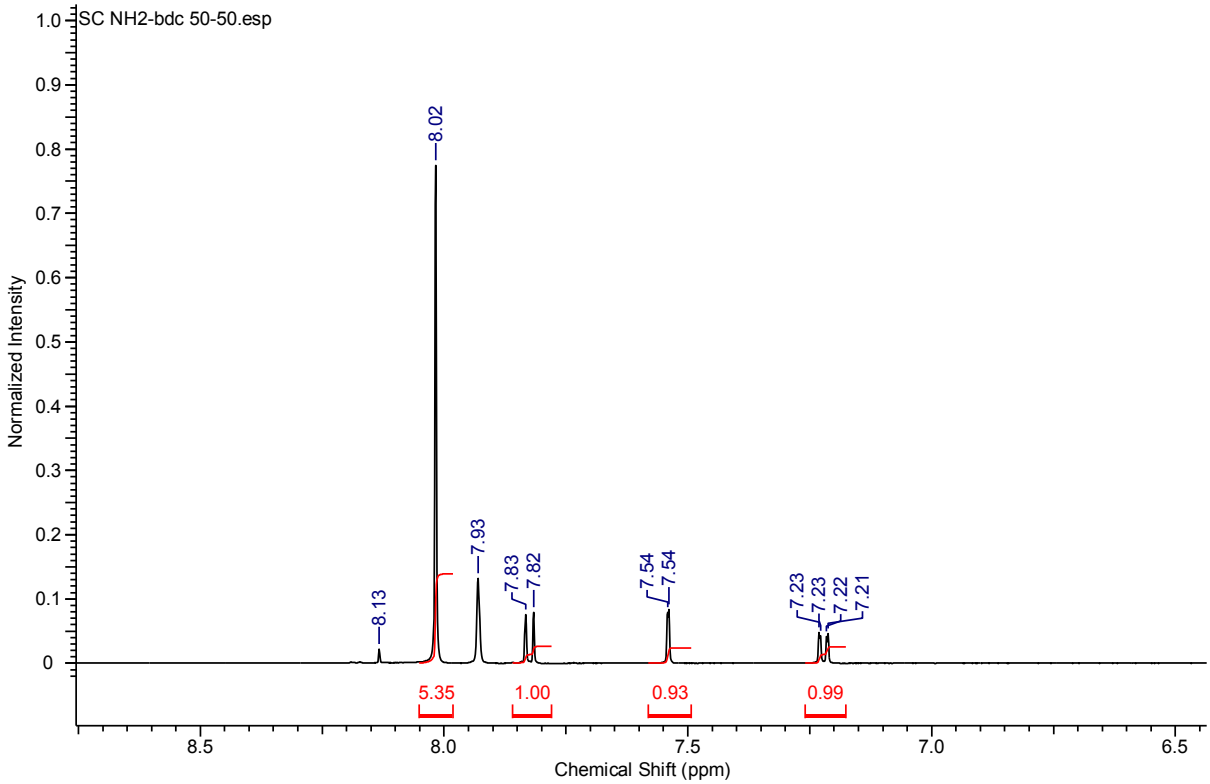

Figure S15. ^{1}H NMR spectrum for a digested single crystal sample of $[Zn_2(bdc)_{1.12}(bdc\text{-}NH_2)_{0.88}(dabco)]\cdot n$DMF

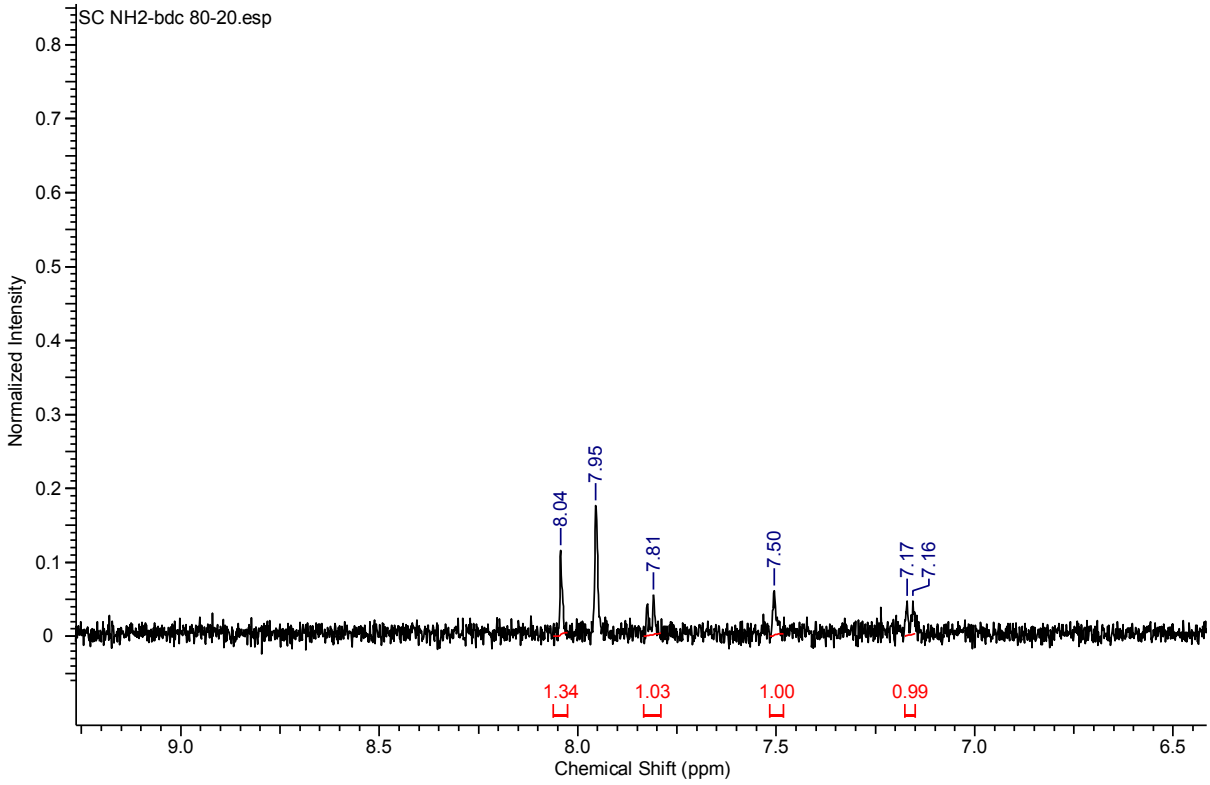

Figure S16. ^{1}H NMR spectrum for a digested single crystal sample of $[Zn_2(bdc)_{0.5}(bdc\text{-}NH_2)_{1.5}(dabco)]\cdot n$DMF

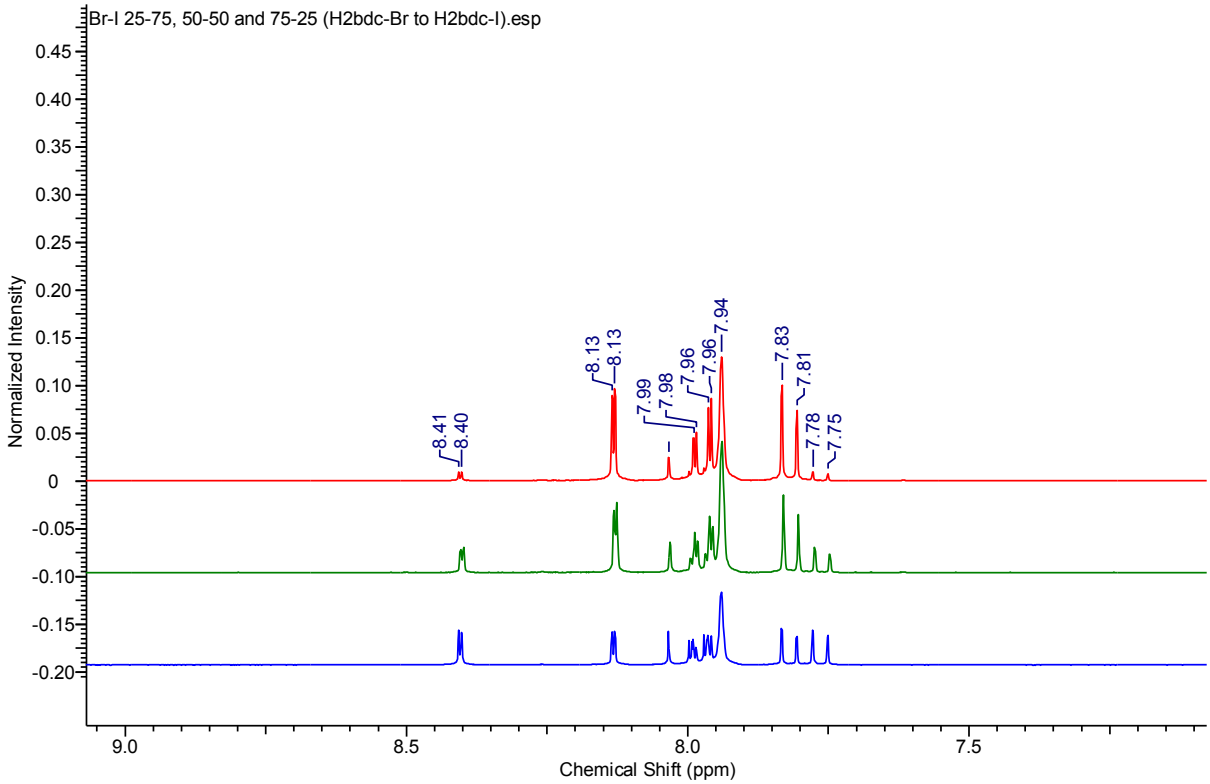

Figure S17. ^{1}H NMR spectrum for the digested bulk samples of all members of the $[Zn_2(bdc\text{-}Br)_{2-x}(bdc\text{-}I)_x(dabco)]\cdot n$DMF (**5**) series

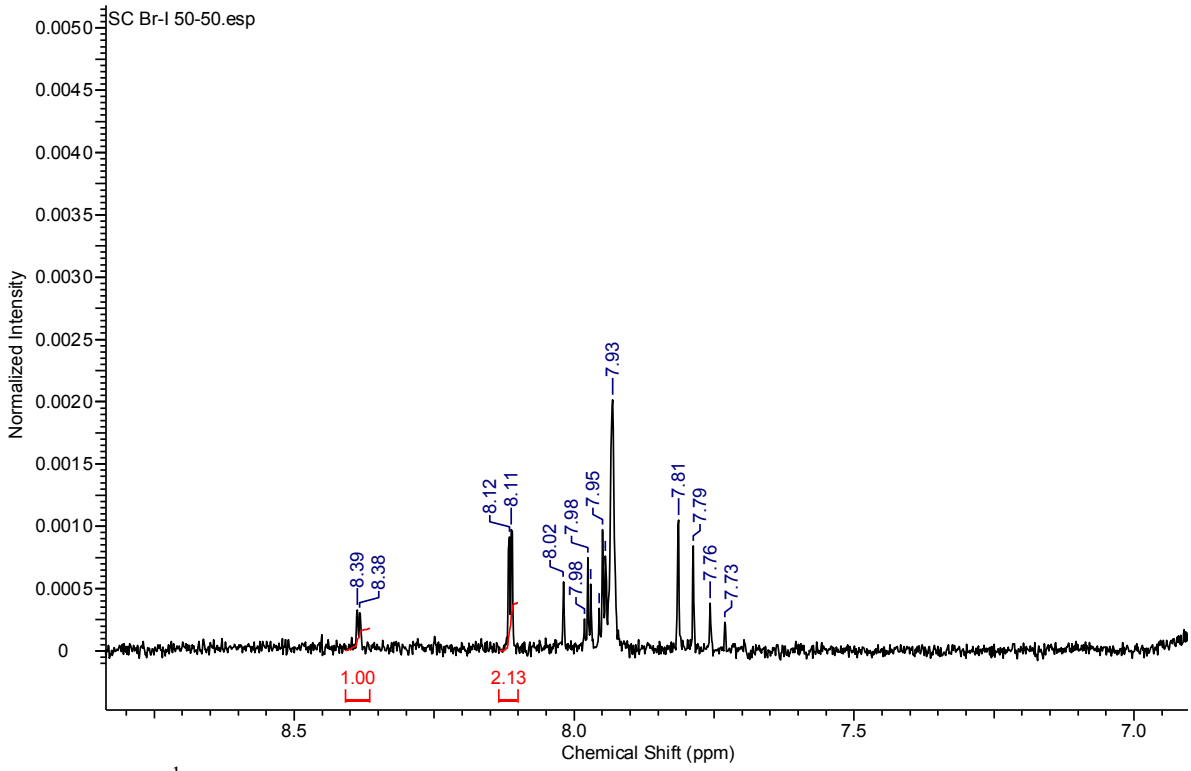

Figure S18. ^{1}H NMR spectrum for a digested single crystal sample of $[Zn_2(bdc\text{-}Br)_{1.42}(bdc\text{-}I)_{0.58}(dabco)]\cdot n$DMF

5. Powder X-ray diffraction studies

The pore geometry of $[Zn_2(bdc)_{2-x}(bdc\text{-}NH_2)_x(dabco)]\cdot n$DMF **4** was unaffected by the value of x, as demonstrated by the X-ray powder diffraction patterns shown in Figure S19.

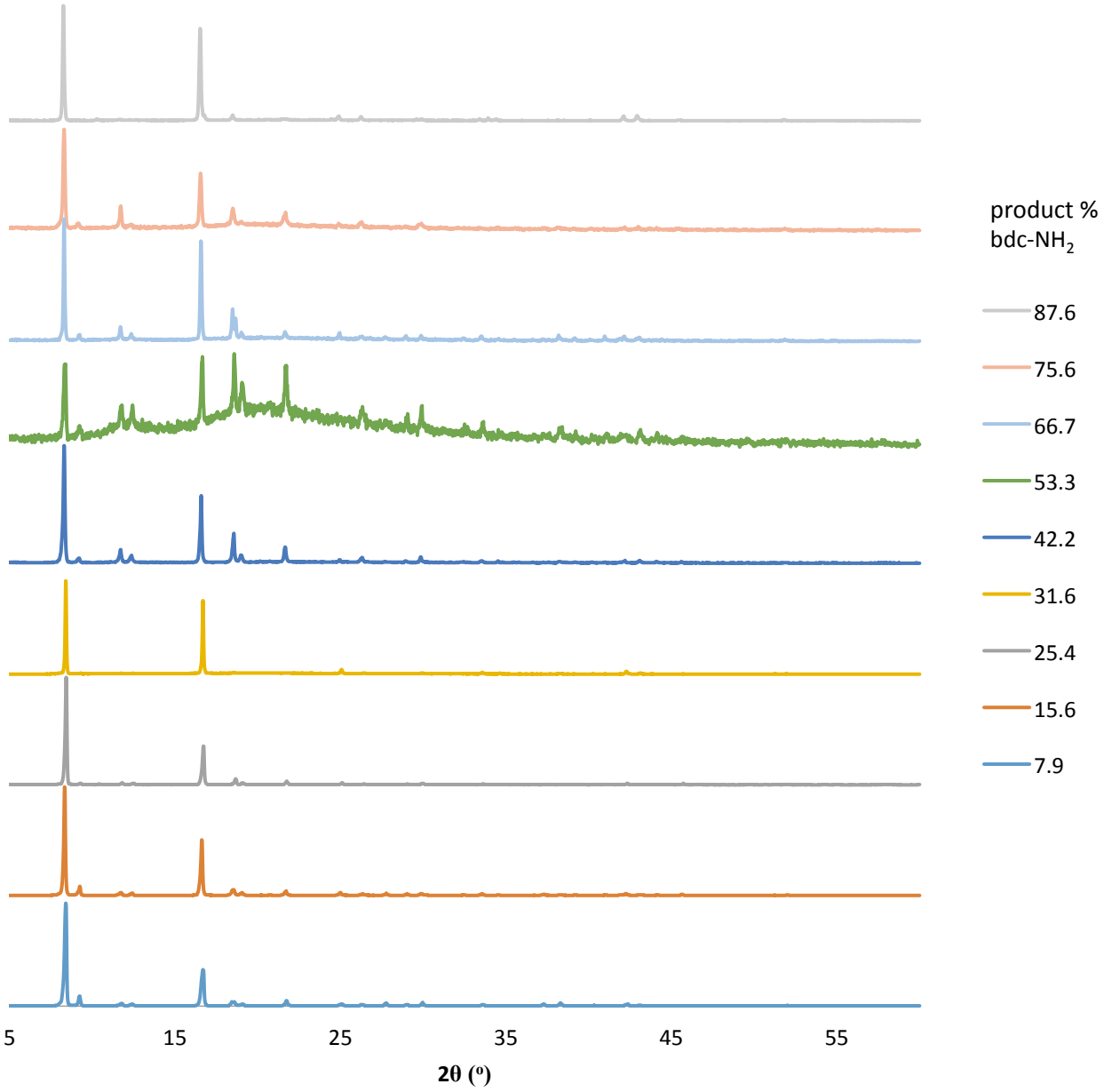

Figure S19. PXRD patterns of the as-synthesised compounds $[Zn_2(bdc)_{2-x}(bdc\text{-}NH_2)_x(dabco)]\cdot n$DMF **4**.

The pore geometry of $[Zn_2(bdc\text{-}Br)_{2-x}(bdc\text{-}I)_x(dabco)]\cdot n$DMF **5** was unaffected by the value of x, as demonstrated by the X-ray powder diffraction patterns shown in Figure S20.

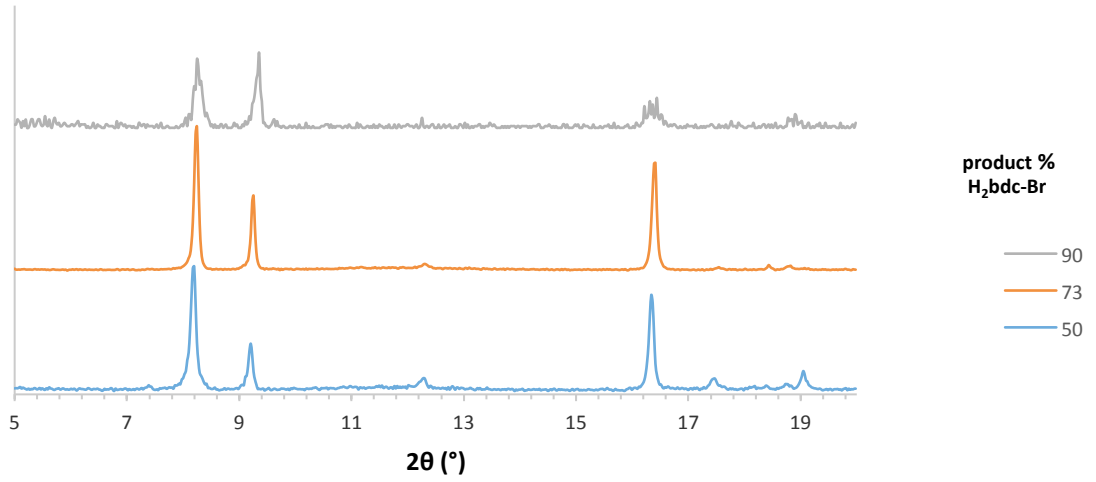

Figure S20. PXRD patterns of the as-synthesised compounds $[Zn_2(bdc\text{-}Br)_{2-x}(bdc\text{-}I)_x(dabco)]\cdot n$DMF **5**.

Figures S21-S28 show the comparison of experimental PXRD patterns to those predicted by corresponding single crystal X-ray crystal structures for the same compound.

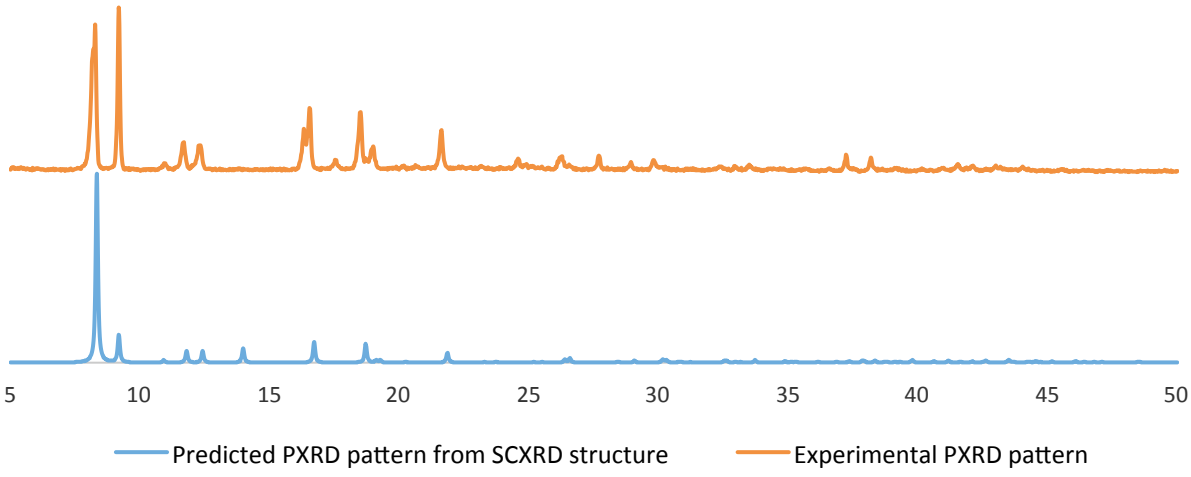

Figure S20. Predicted and experimental PXRD patterns of $[Zn_2(bdc)(bdc\text{-}Br)(dabco)]\cdot n$DMF **1a**.

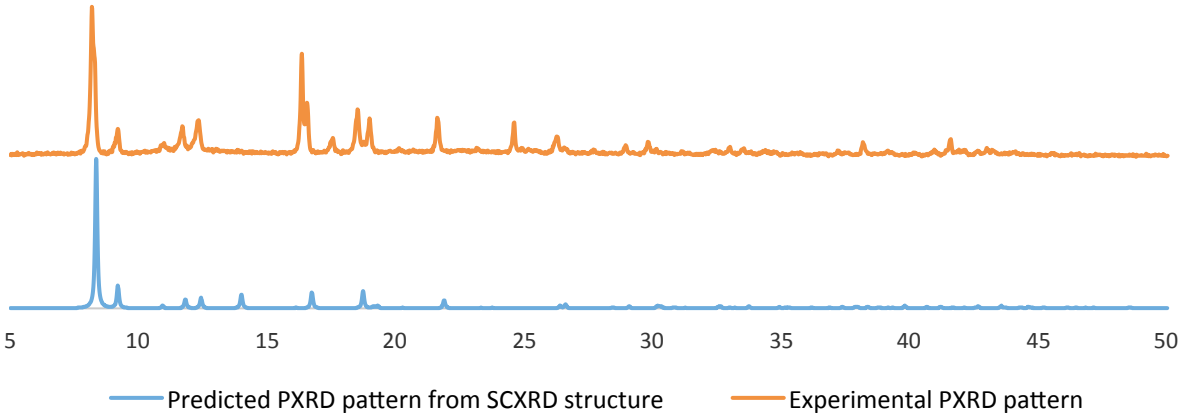

Figure S21. Predicted and experimental PXRD patterns of $[Zn_2(bdc)_{0.8}(bdc\text{-}Br)_{1.2}(dabco)]\cdot n$DMF **1b**.

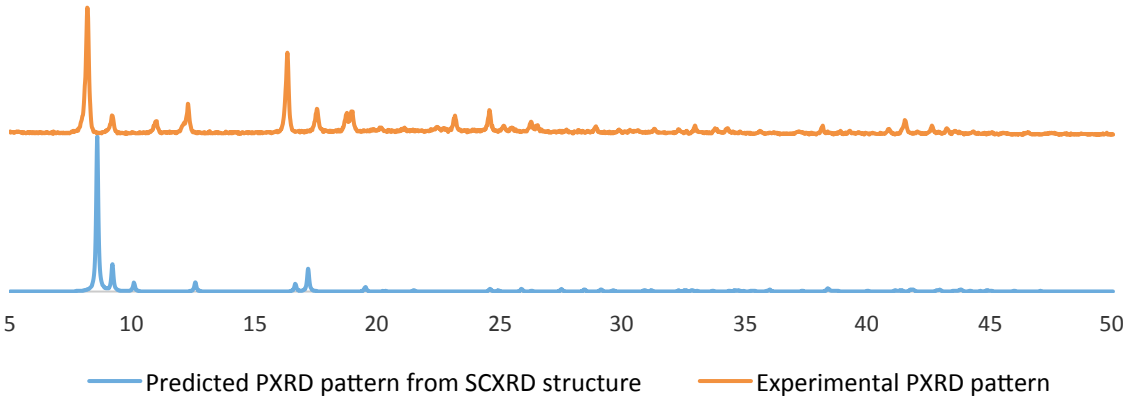

Figure S22. Predicted and experimental PXRD patterns of $[Zn_2(bdc)_{0.4}(bdc\text{-}Br)_{1.6}(dabco)]\cdot n$DMF **1c**. See below.

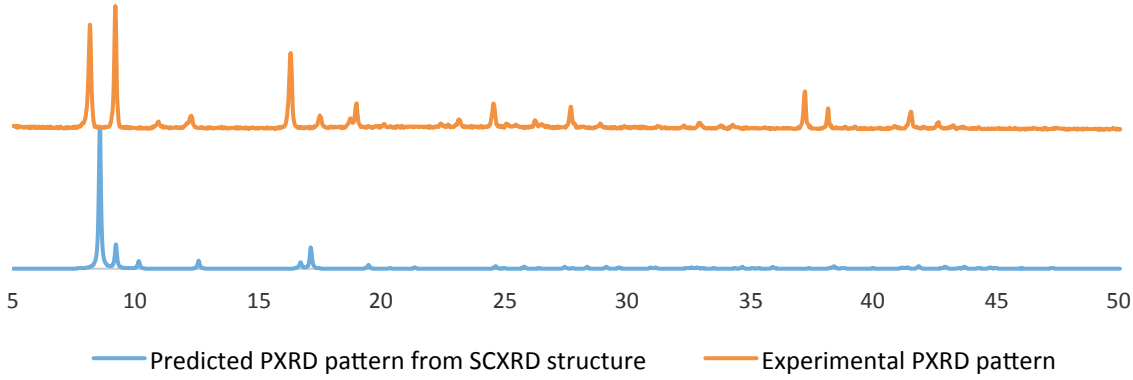

Figure S23. Predicted and experimental PXRD patterns of $[Zn_2(bdc)_{0.3}(bdc\text{-}Br)_{1.7}(dabco)]\cdot n$DMF **1d**. See below.

The PXRD patterns for series **1** show a difference in intensities of some of the peaks between experimental and predicted diffraction patterns. This can be rationalised to some extent by solvent contributions. Solvent treated with "SQUEEZE" does not contribute to the intensities computed via single crystal data. By placing electron density within the pores of the single crystal model, the peak intensities of the predicted powder diffraction patterns can be significantly altered. Additionally, some preferred orientation effects may contribute to intensity differences, as PXRD data were obtained in flat plate mode.

Figures S22 and S23 show relatively poor matches between the experimental powder diffraction patterns and those calculated from the low temperature single crystal structures for **1c** and **1d**. As shown in Figure S24, these is a much better match with the room temperature phase **1c'**.

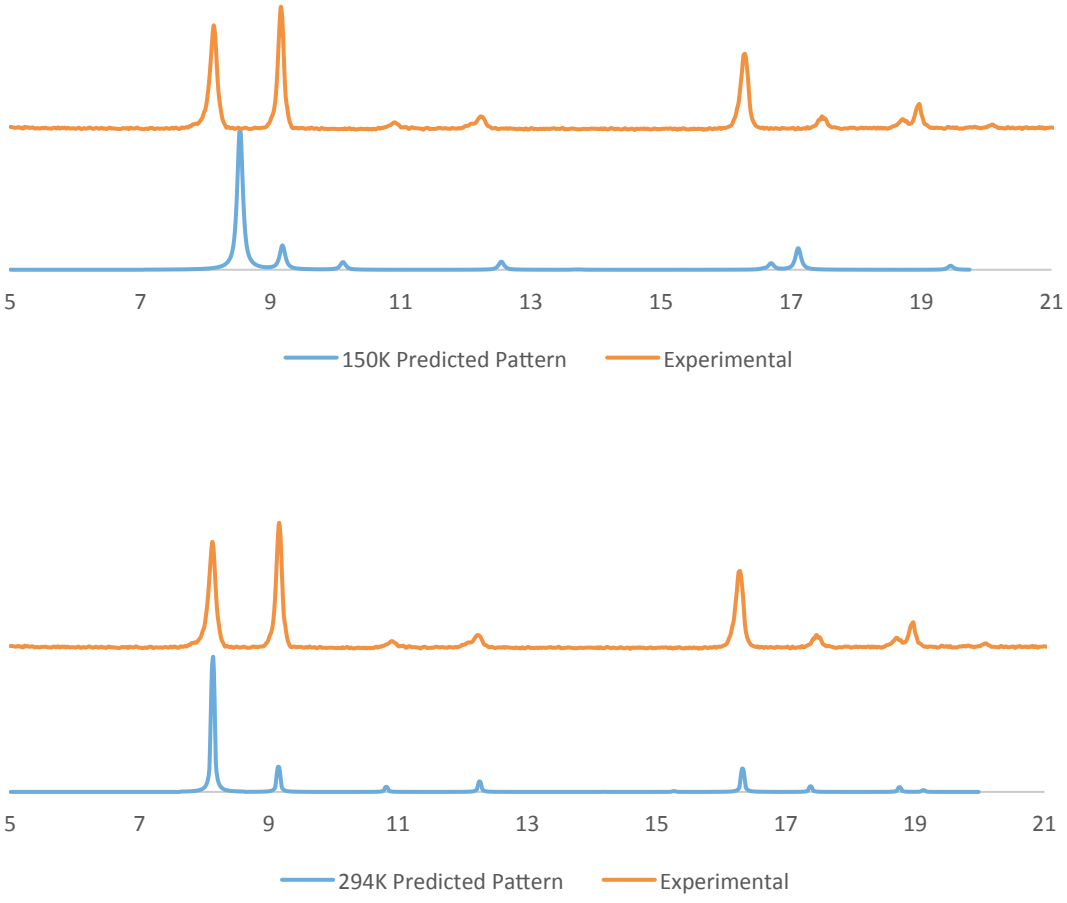

Figure S24. Experimental PXRD patterns of $[Zn_2(bdc)_{0.27}(bdc\text{-}Br)_{1.73}(dabco)]\cdot n$DMF compared to the predicted pattern from single crystal data collections at 150 K **1c** (top) and 298 K **1c'** (bottom)

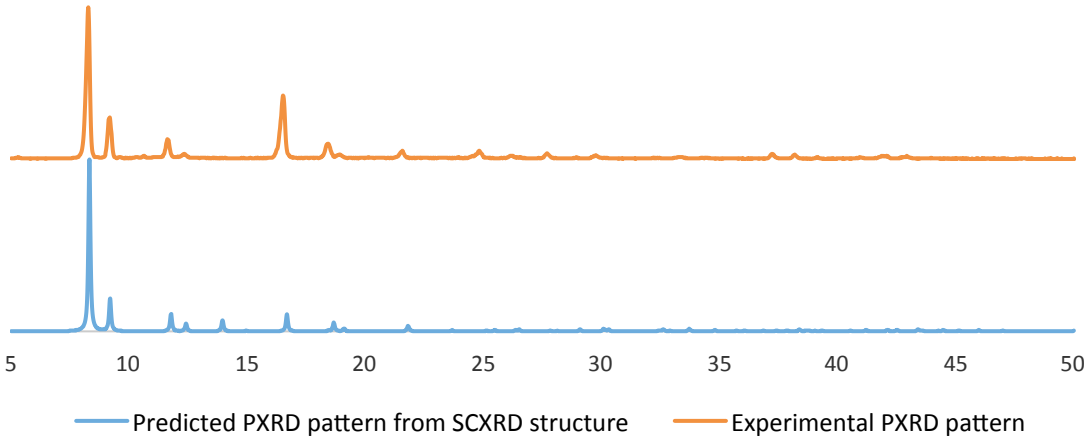

Figure S25. Predicted and experimental PXRD patterns of $[Zn_2(bdc)_{1.2}(bdc\text{-}NO_2)_{0.8}(dabco)]\cdot n$DMF **3a**.

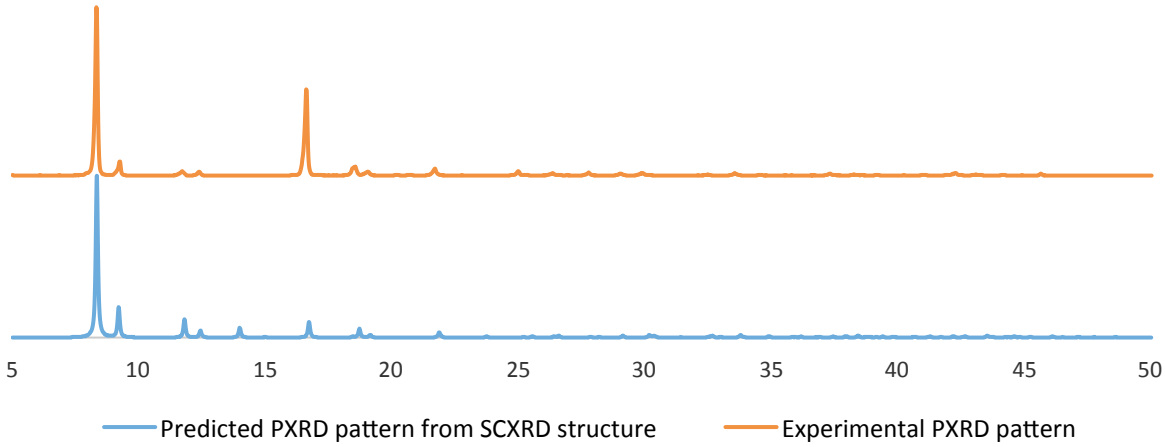

Figure S26. Predicted and experimental PXRD patterns of $[Zn_2(bdc)_{1.6}(bdc\text{-}NH_2)_{0.4}(dabco)]\cdot n$DMF **4a**.

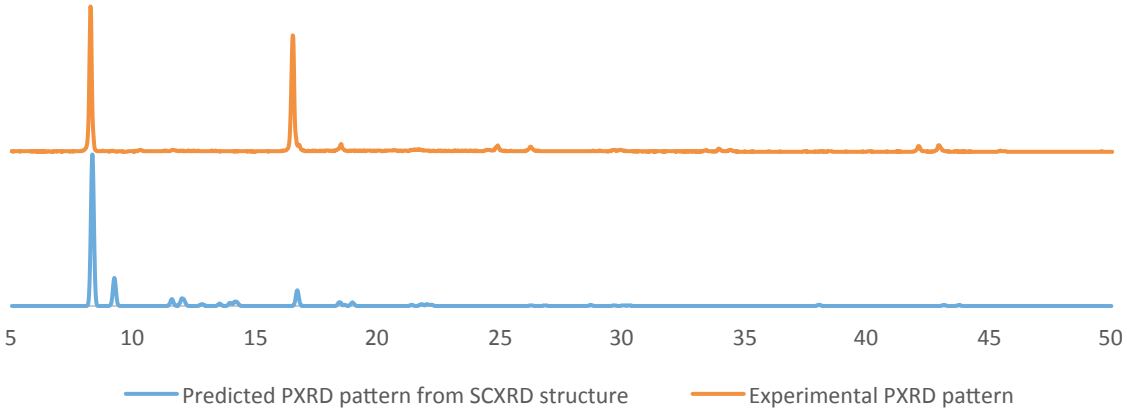

Figure S27. Predicted and experimental PXRD patterns of $[Zn_2(bdc)_{0.2}(bdc\text{-}NH_2)_{1.8}(dabco)]\cdot n$DMF **4b**.

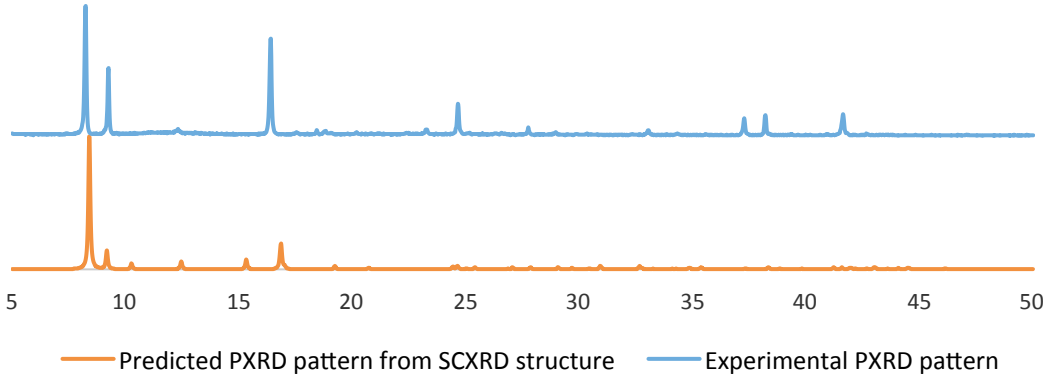

Figure S28. Predicted and experimental PXRD patterns of $[Zn_2(bdc\text{-}Br)_{1.4}(bdc\text{-}I)_{0.6}(dabco)]\cdot n$DMF.

The stabilities of the compounds **1a**, **2a**, **3a**, **4c** and **5a** to air were assessed by PXRD, with diffraction patterns recorded on samples over the course of several weeks. The results are shown in Figures S29-S33 respectively.

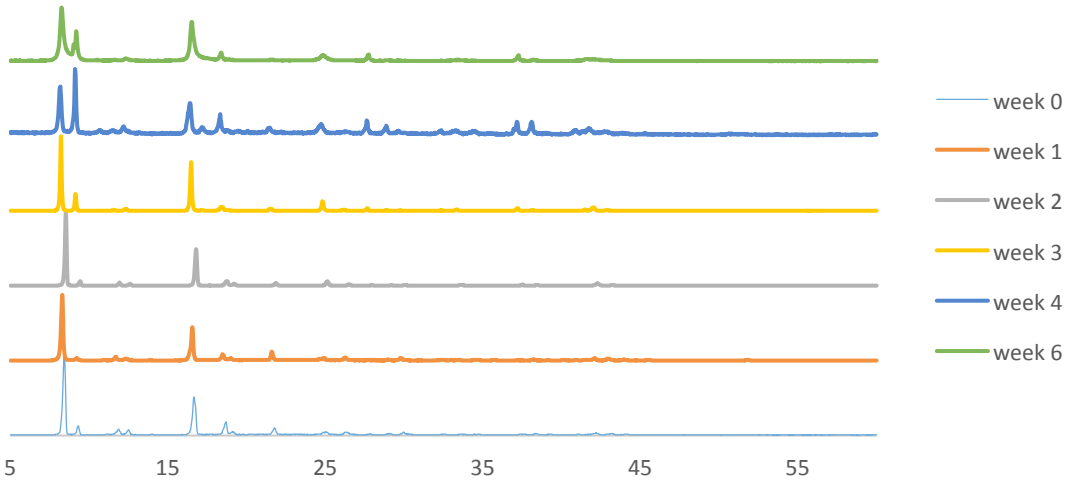

Figure S29. PXRD patterns of $[Zn_2(bdc)(bdc\text{-}Br)(dabco)]\cdot$DMF **1a** left in air over a period of six weeks

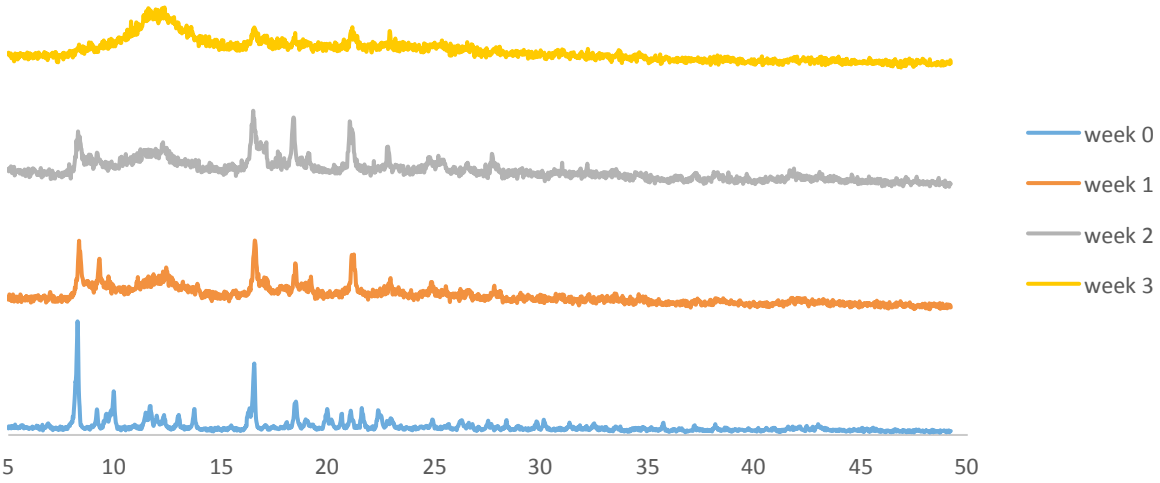

Figure S30. PXRD patterns of $[Zn_2(bdc)_{1.48}(bdc\text{-}I)_{0.52}(dabco)]\cdot n$DMF **2a** left in air over a period of 3 weeks.

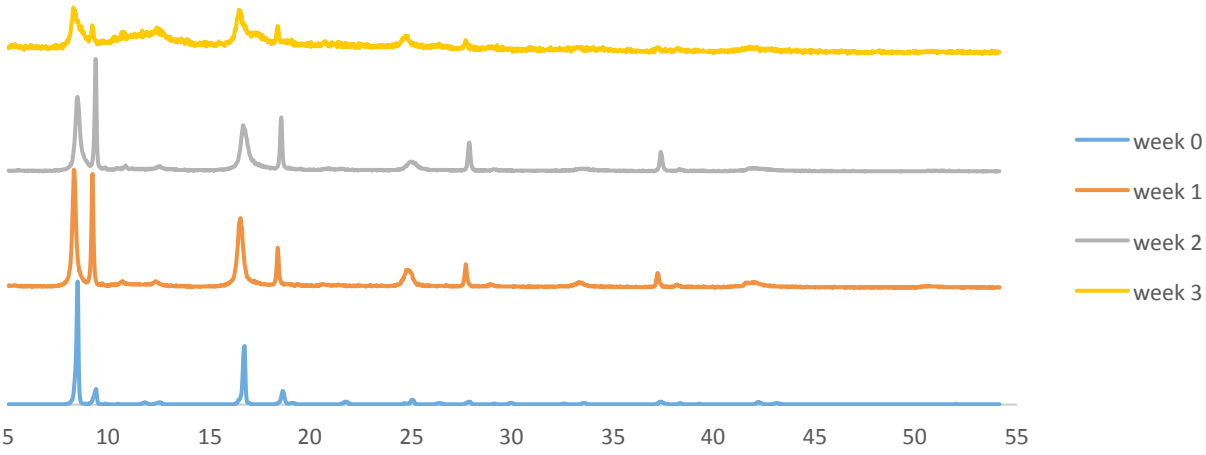

Figure S31. PXRD patterns of $[Zn_2(bdc)_{1.2}(bdc\text{-}NO_2)_{0.8}(dabco)]\cdot 2.5$DMF **3a** left in air over a period of 3 weeks.

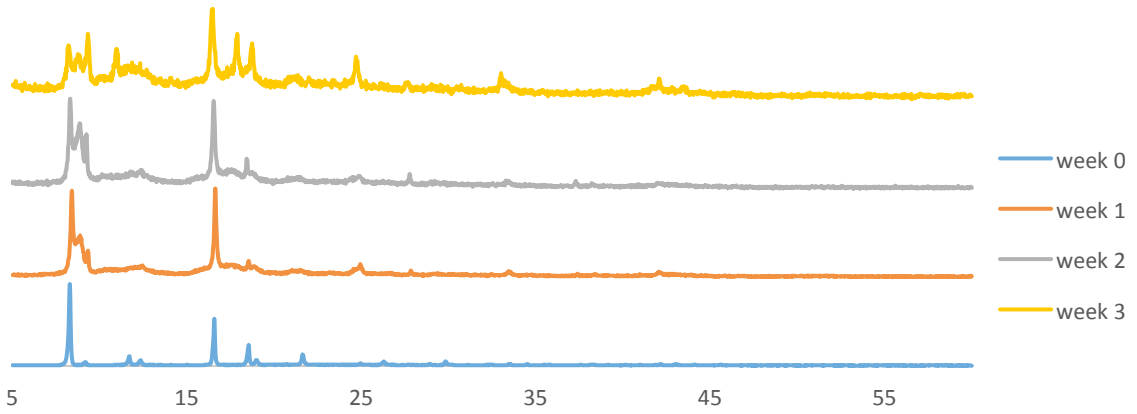

Figure S32. PXRD patterns of $[Zn_2(bdc)_{1.16}(bdc\text{-}NH_2)_{0.84}(dabco)]\cdot n$DMF **4c** left in air over a period of 3 weeks

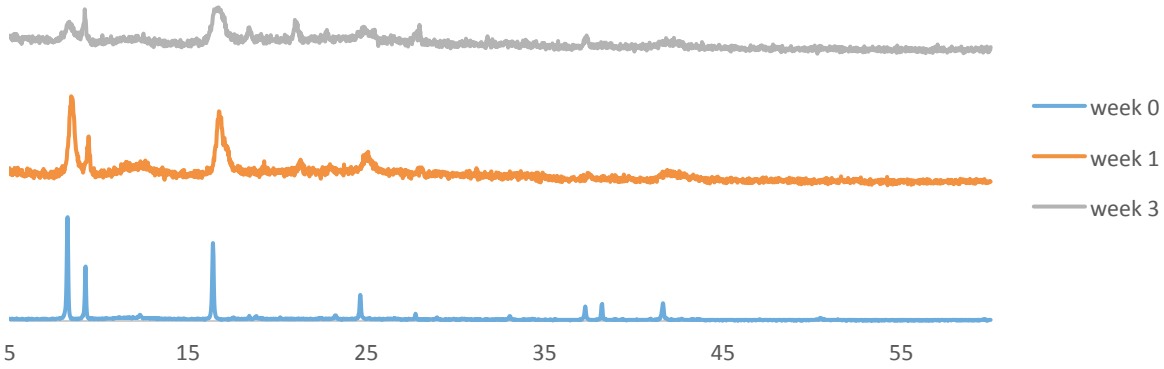

Figure S33. PXRD patterns of $[Zn_2(bdc\text{-}Br)_{1.4}(bdc\text{-}I)_{0.6}(dabco)]\cdot 2.6$DMF **5a** left in air over a period of 3 weeks

Figure S34 shows a comparable analysis of the stability of $[Zn_2(bdc\text{-}Br)_2(dabco)]$ to air.

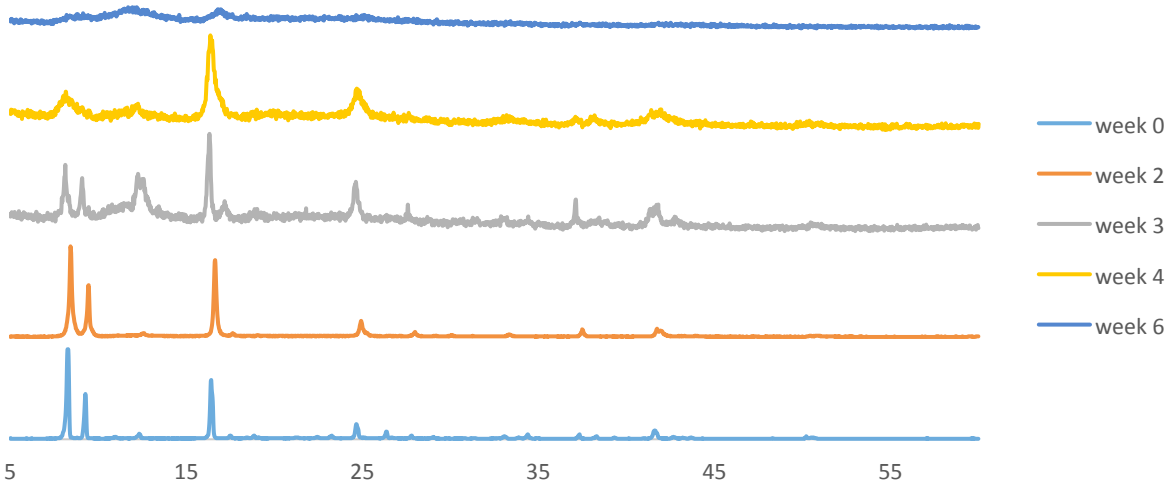

Figure S34. PXRD patterns of $[Zn_2(bdc\text{-}Br)_2(dabco)]$ left in air over a period of 6 weeks.

6. X-ray crystallography

Single crystals of compounds **1a-1d, 3a** and **5a** were analysed on a Nonius Kappa CCD diffractometer using Mo(Kα) radiation, while data for **4a**, **4b** and **1c'** were collected using an Agilent SuperNova using Cu(Kα) radiation. All analyses were conducted at 150 K with the exception of **1c'**, which was collected at 298 K.

Details of the data collections, solutions and refinements are given in Table 4. The structures were uniformly solved using SHELXS-97 and refined using full-matrix least squares in SHELXL-97.[S3] Refinements were uneventful and only noteworthy details follow.

The asymmetric unit in compound **1a** was seen to comprise two zinc centres, each with 25% occupancy, half of a benzene dicarboxylate ligand, one quarter of a dabco and a DMF guest molecule with 0.25 occupancy. Atoms Zn1, Zn2, N1 and N2 are located on a special position in the space group, namely, a 4-fold rotation axis. This means that the dabco carbons are disordered by symmetry. They have been modelled as C5-C8, each with 37.5% occupancy. The bromine on the ligand half has 25% occupancy. Hence, per phenyl ring of the ligand, the bromine is disordered over two positions (related by an inversion centre). Overall, this amounts to half of a bromine, which means that 50% of the time the bdc is brominated, and 50% of the time it is not. There is some disorder in the solvent region which could not be modelled. Hence some distance restraints were employed to assist convergence in this region. ADP restraints were also applied to partial occupancy light atoms. There are small solvent accessible regions in this structure. However, the residual electron density did not warrant an attempt at modelling same, or merit treatment with PLATON SQUEEZE, and hence this algorithm was not employed. Following were the results from PLATON for **1a:**

SQUEEZE RESULTS (Version = 30715, Compound **1a**)

loop_

_platon_squeeze_void_nr

_platon_squeeze_void_average_x

```
 _platon_squeeze_void_average_y
 _platon_squeeze_void_average_z
 _platon_squeeze_void_volume
 _platon_squeeze_void_count_electrons
 _platon_squeeze_void_content
  1  0.250  0.750  0.250       46       2 ' '
  2  0.250  0.750 -0.006       51      -3 ' '
  3  0.250  0.750  0.506       52      -3 ' '
  4  0.250  0.750  0.750       41       2 ' '
  5  0.750  0.250  0.750       46       2 ' '
  6  0.750  0.250  0.006       52      -3 ' '
  7  0.750  0.250  0.494       51      -3 ' '
  8  0.750  0.250  0.250       41       2 ' '
_platon_squeeze_void_probe_radius          1.20
```

Refinement of the model for compound **1b,** which contains 60% of the brominated ligand, was quite similar to that for **1a,** down to the indication of some small structural voids. As for **1a** PLATON SQUEEZE was not employed here either – based on the following 'test' results:

```
# SQUEEZE RESULTS (Version =  30715, Compound 1b)
loop_
    loop_
     _platon_squeeze_void_nr
     _platon_squeeze_void_average_x
     _platon_squeeze_void_average_y
     _platon_squeeze_void_average_z
     _platon_squeeze_void_volume
     _platon_squeeze_void_count_electrons
     _platon_squeeze_void_content
      1  0.250  0.750  0.250       36      -1 ' '
      2  0.250  0.750  0.750       36      -1 ' '
      3  0.250  0.750  0.000       56       0 ' '
      4  0.250  0.750  0.500       55       0 ' '
      5  0.750  0.250  0.750       36      -1 ' '
      6  0.750  0.250  0.250       36      -1 ' '
```

```
 7  0.750  0.250  1.000       55        0 ' '
 8  0.750  0.250  0.500       55        0 ' '
_platon_squeeze_void_probe_radius              1.20
```

Once again, in **1c**, the bromine was disordered around the phenyl ring of the ligand, such that the 0.4 of a halide present per half zinc is disordered in a 15:5 ratio between C3 and C3A. Disordered hydrogen atoms in this phenyl moiety could not be reliably located and hence were omitted from the refinement. The asymmetric unit in the structure was seen to contain one quarter of a zinc centre, one quarter of a dabco moiety, and one quarter of a benzene dicarboxylate ligand, with N1, C1, C2, C5 and Zn1 located at special positions. This necessarily means that the dabco carbons (C4 and C5) are disordered over 2 sites. ADP restraints applied to some partial occupancy atoms to assist convergence.

Refinement of the model for structure **1d** presented similar issues to that for **1c**. The only point meriting note is that the 0.2125 bromine present in the asymmetric unit of **1d** is disordered in a 16.25:5 ratio between C3 and C3A. It is likely that there is a small amount of diffuse solvent present in the framework pores of **1c** and **1d**. However, analysis using PLATON SQUEEZE suggested that this was minimal – although said findings from PLATON are not optimally reliable owing to the disorder of the ligand phenyl ring over 2 sites coupled with the bromine disorder. The 'test' results from PLATON SQUEEZE follow for **1c** and **1d**, respectively:

```
# SQUEEZE RESULTS (Version =  30715; Compound 1c)
loop_
 _platon_squeeze_void_nr
 _platon_squeeze_void_average_x
 _platon_squeeze_void_average_y
 _platon_squeeze_void_average_z
 _platon_squeeze_void_volume
 _platon_squeeze_void_count_electrons
 _platon_squeeze_void_content
  1 -0.058  0.000  0.000       248        20 ' '
  2 -0.055  0.500  0.500       248        20 ' '
_platon_squeeze_void_probe_radius              1.20


# SQUEEZE RESULTS (Version =  30715; Compound 1d)
loop_
 _platon_squeeze_void_nr
 _platon_squeeze_void_average_x
```

```
 _platon_squeeze_void_average_y
 _platon_squeeze_void_average_z
 _platon_squeeze_void_volume
 _platon_squeeze_void_count_electrons
 _platon_squeeze_void_content
  1 -0.053  0.000  0.000       263        9 ' '
  2 -0.048  0.500  0.500       263        9 ' '
_platon_squeeze_void_probe_radius              1.20
```

The structure of compound **1c'** represents a room temperature data collection on a sample from the batch of **1c**. The optimal refinement was attained by modelling the bromine as being disordered around the phenyl ring of the ligand, such that the 0.76 bromine present per one zinc is disordered in a 0.135:0.055 ratio between the half occupancy C3 and C3A. Disordered hydrogen atoms in this phenyl moiety could not be reliably located and hence were omitted from the refinement. Zn1, N1, and C6 are located at special positions in the space group and as for the low temperature data collection, this necessarily means that the dabco carbons are disordered. These were modelled as C4, C5 and C6, with occupancies of 0.305, 0.305 and 0.28, respectively. ADP restraints were applied to these partial occupancy carbon atoms to assist anisotropic convergence. While there is some void space in the structure, analysis from SQUEEZE suggests very little electron density. This aligns with the evidence in the difference Fourier map and, hence, the SQUEEZE data were not employed in this refinement. The results from PLATON SQUEEZE for **1c'** were as follows:

```
# SQUEEZE RESULTS
loop_
 _platon_squeeze_void_nr
 _platon_squeeze_void_average_x
 _platon_squeeze_void_average_y
 _platon_squeeze_void_average_z
 _platon_squeeze_void_volume
 _platon_squeeze_void_count_electrons
 _platon_squeeze_void_content
  1 -0.088  0.500  0.000       255        9 ' '
  2 -0.078  0.000  0.500       255        9 ' '
_platon_squeeze_void_probe_radius              1.20
```

Compound **3a** has an asymmetric unit containing one quarter of a zinc atom, one quarter of a dabco ligand, one quarter of a bdc ligand (comprised of a 40:60 bdc-NO_2:bdc ratio) and some guest solvent. Zn1 and the dabco nitrogen (N2) lie on a crystallographic 4-fold rotation axis. The nitro moiety from the functionalised bdc ligand was seen to be disordered around all four phenyl carbons of the linker. As the structure is of high symmetry, this necessarily means that

the nitrogen atom (N1), therein, is present in the asymmetric unit at 15% occupancy. The associated ADP was consequently refined with some restraints, and subject to this low occupancy fractional atom being at a distance of 1.38(2) Å from the carbon atom to which it is bound. Moreover, the two oxygen atoms bonded to N1 could not be located with certainty and hence were omitted from the model - although there was electron density evident in the expected region of the difference Fourier electron density map. The dabco carbons also exhibited disorder which resulted in refinement of C4 and C5 with 0.35 and 0.40 occupancies, respectively, and with some ADP restraints to assist convergence. Guest solvent was diffuse and was treated with the PLATON SQUEEZE algorithm. However, a quantity of 2.5 DMF molecules per pair of zinc centres has been accounted for in the formula as presented. This was determined primarily by TGA on the bulk sample.

Crystals of **3b** were of poor quality and suffered from extensive disorder. While the solution is not of sufficient quality to present in full, it is notable that **3b** crystallises in an orthorhombic system, similar to **1b**, **1c** and **5a**, with space group *C*222. The unit cell parameters are a = 12.871(9) Å, b = 17.4764(11) Å and c = 9.6458(5) Å.

The asymmetric unit in **4a** was seen to be composed of two zinc centres (each with 25% occupancy), half of a dicarboxylate ligand and two dabco fragments (each comprising one nitrogen with 25% occupancy and 2 fractional occupancy (0.375) carbon atoms). As for **1a** and **1b**, atoms with 25% occupancy in **4a** are coincident with a crystallographic 4-fold rotation axis. The dicarboxylate ligand present is an average of 20% bdc-NH_2 and 80% bdc. The amino group is disordered between C5 and C6 in in a 35:65 ratio. Associated C–N distances pertaining to the amino nitrogen atoms were restrained and these low occupancy partial nitrogen atoms were refined subject to lying in the same plane as the other ligand atoms. Disorder was also prevalent with respect to the dabco carbon atoms which were each modelled at two positions as indicated above, with included ADP restraints, to assist convergence. There was evidence for some diffuse solvent in the lattice pores, but this could not be modelled credibly. Hence, it was treated via PLATON-SQUEEZE. Based on the pre-SQUEEZE difference Fourier electron density map, the findings from this algorithm and TGA results, 1.3 molecules of DMF has been included per metal centre in the empirical formula given in Table 4.

In **4b**, the asymmetric unit was seen to consist of one zinc centre, one dicarboxylate ligand and half of a dabco moiety. The dicarboxylic ligand is an average of 90% bdc-NH_2 and 10% bdc. The amino group disordered between C7, C3 and C4 in a 40:10:40 ratio. C-N distances pertaining to the amino nitrogens were restrained to being similar. Disorder was also prevalent with respect to the three dabco carbon atoms which were each modelled at two positions in a 50:50 ratio. As for **4a** some ADP restraints were applied to these fractional occupancy carbon atoms, to improve convergence. Diffuse pore solvent was treated via PLATON-SQUEEZE and 0.75 molecules of DMF has been included per metal centre in the empirical formula for this MOF based on similar considerations to those employed for **4a**.

The asymmetric unit in **5a** was seen to incorporate half of a zinc atom, half of a dabco ligand, half of a bdc ligand (comprised of a 30:70 bdc-I:bdc-Br ratio) and some guest solvent. Zn1 and the dabco nitrogen (N1) are co-incident with a crystallographic 2-fold rotation axis. Unsurprisingly, the halide substituents in the functionalised bdc ligand mixture present were seen to be disordered around all four phenyl carbons of the linker. As the asymmetric unit contains half of a phenyl ring from the linker, this means that both the iodine and bromine are

disordered in terms of attachment to the carbons at the 2-position. However, each of these carbons exhibited 65:35 disorder. Consequently, the electron density pertaining to the halides was quite smeared. Additionally, the bromine and iodine were seen to be disordered between the 2 carbons available to them in a 30:5 and 12:3 ratios, respectively. Overall, this model needed a moderate number of ADP and distance restraints to assist convergence as a result of disorder and the level of diffraction from the sample. The dabco carbons exhibited disorder which is not surprising as this entity does not have 2-fold rotational symmetry along the N···N vector. Thus, C5, C6 and C7 were each refined with 50% site occupancy. The hydrogen atoms pertaining to the bdc ligands were not included because of the halide disorder. Guest solvent was diffuse and was treated with the PLATON SQUEEZE algorithm. However, a quantity of 2.6 DMF molecules per pair of zinc atoms has been accounted for in the formula as presented in Table 4. This was determined primarily by TGA data on the bulk sample.

7. Computational Methodology

Electronic structure calculations were carried out on the periodic crystals in the VASP (Vienna *ab-initio* Simulation Programme) code. The PBEsol functional was used to calculate the electronic density distribution within the systems. PBEsol is known to accurately reproduce the structural and electronic properties of solid-porous materials.[S4] Γ-point calculations were conducted on all structures due to large unit-cell lengths and sufficient sampling sizes. The quasi-Newtonian relaxation employed for structural optimization was converged to forces of 0.005 eV/Å or lower and kinetic energy cut-off of 500 eV was employed for the basis set. To model the interactions between core and shell of the atoms, projector-augmented wave (PAW) potentials were used.[S5]

To calculate the MEP (minimum energy path) for each structural transformation, SS-NEB (solid-state nudged elastic band) calculations were performed also using the VASP code.[S6, S7] It is necessary to use the solid-state correction of the nudged elastic band model to include changes in unit-cell volume during a phase transition. The SS-NEB is a contribution to the VASP code by Henkelman *et al.* and requires single point calculations to be performed on each image generated by a linear interpolation between the two optimised initial and final structures (before and after the phase change). Forces are calculated by projecting the perpendicular component of the force acting upon each image allowing the MEP (minimum energy path) between the generated images to be calculated. The climbing image nudged elastic band (CI-NEB) profiles are reported to demonstrate the 'true' maxima of the highest energy image generated by the nudged elastic band method.[S8] The number of images are an important consideration to ensure the highest energy image structural configuration is representative of the 'true' saddle point. Considering computational expense and accuracy, 24 images were created for each calculation. The number of images chosen represents a high accuracy for plotting a MEP for such a structural transformation.

The program critic2[S9, S10] was used to study the chemical interactions within the non covalent interactions (NCI) methodology. NCI index identifies interactions in a chemical system analysing the electron density (ρ) and its reduced gradient:

$$s = \frac{1}{2(3\pi^2)^{\frac{1}{3}}} \frac{|\nabla\rho|}{\rho^{\frac{4}{3}}}$$

NCIplot within VMD was then used to visualise charge density associated with non-covalent interactions such as dispersion between two non-bonded species.[S11, S12]

8. References

S1 A. Kommreddy, M. S. Bowsher, M. R. Gunna, K. Botha and T. K. Vinod, *Tetrahedron Lett.*, 2008, **49**, 4378.

S2 D. N. Dybtsev, H. Chun and K. Kim, *Angew. Chem. Int. Ed.*, 2004, **43**, 5033.

S3 G. M. Sheldrick, *Acta Cryst.* 2008, **A64**, 112.

S4 J. P. Perdew, K. Burke and M. Ernzerhof, *Phys. Rev. Lett*, 1996, **77**, 3865.

S5 P. E. Blöchl, *Phys. Rev. B*, 1994, **50**, 17953.

S6 G. Henkelman and H. Jónsson *J. Chem. Phys.,* 2000, **113**, 9978.

S7 G. Henkelman, B. P. Uberuaga and H. Jónsson, *J. Chem. Phys.*, 2000, **113**, 9901.

S8 K. J. Caspersen and E. A. Carter. *Proc. Natl. Acad. Sci USA,* 2005, **102**, 6738.

S9 A Otero de la Roza, E. R. Johnson and V. Luaña. *Comput. Phys. Commun.,* 2014, **185**, 1007.

S10 A Otero de la Roza, *Comput Phys. Commun.,* 2009, **180**, 157.

S11 J. Contreras-Garcia, E. R. Johnson, S. Keinan, R. Chaudret, J. P. Piquemal, D. N. Beratan and W. Yang, *J .Chem. Theory Comp.*, 2011, **7**, 625.

S12 W. Humphrey, A. Dalke and K. Schulten. *J. Mol. Graphics* 1996, **14**, 33.